On parallel simulation of a new linear Cosserat elasticity model with grid framework model assumptions

Hamidréza Ramézani, Jena Jeong, Zhi-Qiang Feng

On parallel simulation of a new linear Cosserat elasticity model with grid framework model assumptions

Hamidréza Ramézani [a,*], Jena Jeong [b,*], Zhi-Qiang Feng [c,d,1]

[a]CRMD, UMR CNRS 6619-Research Center on Divided Materials, École Polytechnique de l'Université d'Orléans, 8 rue Léonrad de Vinci, 45072 Orléans Cedex 2, France

[b]ESTP/IRC/LM-Lean Modeling-École Spéciale des Travaux Publics, du Bâtiment et de l'industrie (ESTP), 28 Avenue du Président Wilson, 94234 Cachan Cedex, France

[c]School of Mechanics and Engineering, Southwest Jiaotong University, Chengdu, China

[d]LMEE, EA 3332-Laboratoire de Mécanique et Énergétique, Université d'Evry-Val d'Essonne, 40, Rue du Pelvoux, 91020 Evry Cedex, France

In the present paper, the linear Cosserat elasticity involving the grid framework model for micro-rotations as boundary condition or side-condition has been taken into account. The identical micro-rotation constants $\left(\alpha=\beta=\gamma=\mu L_c^2 \text{ or } \Psi=\frac{2}{3}\right)$ assumption or so called case 4, altogether case 1 ($\alpha=\beta=0$ and $\gamma=\mu L_c^2$), case 2 $\left(\alpha=0 \text{ and } \beta=\gamma=\frac{1}{2}\mu L_c^2\right)$ and conformal case 3 $\left(\alpha=-\frac{1}{3}\mu L_c^2 \text{ and } \beta=\gamma=\frac{1}{2}\mu L_c^2\right)$ are examined by means of some numerical experiments for torsion test with a circular bar. The presence of m_{33} (stress moment in z direction) on the top of specimen is confirmed numerically and analytically via a missing term $\left(\int_{\partial\Omega_t}(r\times t^{(n)})\cdot\delta\phi\, dS\right)$. By considering this term, m_{33} is non-zero, whereas, the Dirichlet boundary condition for displacements on the top of bar is used to apply the torque (M_T). The outcomes reveal that the case 4 as well as other cases is still bounded. This property is found out for curvature stiffness as well. These cases are presented in *Torque*-Log (L_c) diagram. In this diagram, two non-size affected zones (zones I and III) and one size affected zone would be inferred. By taking advantage of this curve, we can probably consider Cosserat theory as a multi-scale tool and some outlooks for a fresh experimental departure are discussed.

1. Introduction

1.1. Overview

This article addresses a novel linear Cosserat model involving the grid framework model assumption [1,2]. We have investigated another interesting case (case 4) in which identical micro-rotation constants are used $\left(\alpha=\beta=\gamma=\mu L_c^2 \text{ or } \Psi=\frac{2}{3}\right)$. The numerical outcomes show that all mentioned cases are bounded whatever L_c values [3–5]. Furthermore, the curvature stiffness torque is bounded as well as stiffness torque including the Dirichlet boundary conditions for displacements and

* Corresponding authors. Tel.: +33 2 38 257879; fax: +33 2 38 255376 (H. Ramézani), tel.: +33 1 49 082303; fax: +33 1 45 476039 (J. Jeong).

E-mail addresses: hamidreza.ramezani@univ-orleans.fr, hamidreza.ramezzani@gmail.com (H. Ramézani), jeong@profs.estp.fr, jena.jeong@gmail.com (J. Jeong), feng@iup.univ-evry.fr (Z.-Q. Feng).

[1] Tel.: +33 1 69 477501; fax: +33 1 69 477599.

Nomenclature

Constants

α	first micro-rotation or micro-rotation constant in [N]
β	second micro-rotation or micro-rotation constant in [N]
ℓ_1, ℓ_2 and ℓ_3	first, second and third characteristic length scale [m]
ℓ_t	characteristic length scale for torsion in [m]
γ	third micro-rotation or micro-rotation constant in [N]
κ	Cosserat couple modulus in accordance with the Eringen's notation in [Pa]
λ	first Lamé's constant in [Pa]
μ	second Lamé's constant in [Pa]
μ^*	Pseudo-Lamé's constant in accordance with the Eringen's notation in [Pa]
μ_c	Cosserat couple modulus in [Pa or N/m^2]
ν	Poisson's ratio in [–]
$\boldsymbol{\Psi}$	polar ratio in [–]
E	Young's modulus in [Pa]
L_c	Cosserat characteristic length scale in [m]
N	coupling number in [–]

Third-rank tensor quantities

e	antisymmetrical permutation tensor or Levi–Civita tensor in [–]

Sets

$\mathbb{M}^{3\times3}$ or $\mathbb{R}^3 \times \mathbb{R}^3$	set of real 3×3 second-rank tensors
$\mathbb{N}$	natural set
$\mathbb{R}$	real set

Second-rank tensor quantities

$-\overline{A}$	dual tensor of the micro-rotation vector [rad.]
$\bar{\varepsilon}$	non-symmetric first Cosserat stretch tensor in [–]
$\bar{\sigma}$	unsymmetrical stress tensor in [Pa]
$\bar{\sigma}_{ij}^{exact}$	exact stress components corrected by deformation gradient tensor on $\partial\Omega_1$ in [Pa]
$\bar{k}$	micropolar curvature tensor in [m^{-1}]
$\bar{k}_{ij}^{\text{skew}}$	skew symmetric counterpart components of the micropolar curvature tensor in [m^{-1}]
$\bar{k}_{ij}^{\text{sym}}$	symmetric counterpart components of the micropolar curvature tensor in [m^{-1}]
$\delta\bar{\varepsilon}$	virtual first Cosserat stretch tensor in [–]
$\delta\bar{k}$	virtual micropolar curvature tensor in [m^{-1}]
$\mathbb{I} = \delta_{ij}\hat{\mathbf{e}}_i \otimes \hat{\mathbf{e}}_j$	identity matrix [–]
∇u	gradient of displacement vector in [–]
B	initial couple stress tensor or so-called stress moment tensor [N m/m^2 or Pa m]
S	initial stress tensor in [Pa]
m_{ij}^{exact}	exact couple stress components corrected by deformation gradient tensor on $\partial\Omega_1$ in [Pa m]
S_1	first Piola–Kirchhoff or 1st P–K stress tensor in [Pa]
T_1	so-called first Piola–Kirchhoff or 1st P–K couple stress tensor in [N m/m^2 or Pa m]
X and Y	arbitrary second-rank tensors
F	deformation gradient tensor in [–]
m	unsymmetrical couple stress or stress moment tensor in [N m/m^2 or Pa m]

Scalar quantities

ΔA	infinitesimal area in [m^2]
ρ	density in [kg/m^3]
ϑ	Geometrically exact angle of rotation in [rad.]
$J = det$[F]	determinant of deformation gradient tensor in [–]
$W(\bar{\varepsilon}, \bar{k})$	total energy density function in [J/m^3]
$W_{\text{cs}}(\bar{\varepsilon}, \bar{k})$	centrosymmetrical energy density in [J/m^3]
W_{cs}^0	initial centrosymmetrical energy density in [J/m^3]
$W_{\text{curv}}(\bar{\varepsilon}, \bar{k})$	curvature energy density in [J/m^3]
W_{curv}^0	initial curvature energy density in [J/m^3]
$W_{\text{mp}}(\bar{\varepsilon}, \bar{k})$	strain energy density in [J/m^3]
W_{mp}^0	initial strain energy density in [J/m^3]

Fourth-rank tensor quantities

$\mathbf{C}$	Centrosymmetrical fourth-rank tensor [N/m]
$\mathbf{D}$	stiffness fourth-rank tensor [Pa]
$\mathbf{E}$	curvature stiffness fourth-rank tensor [N]

Vector quantities

$\bar{\omega}$	macro-rotation in [rad.]
$\overline{Q}^{(n)}$	total surface couple in [N m/m^2 or Pa m]
ΔF	infinitesimal force in [N]
ΔM	infinitesimal moment in [N m]
$\hat{e}_i$	Cartesian unit base vector [–]
ϕ	micro-rotation or micro-rotation vector in [rad.]
ρb	body force in [N/m^3]
ρc	body couple in [N m/m^3]
a, b and x	arbitrary vectors
$M^{exact}_{\mathrm{Tcurv}}$	curvature stiffness-based torque on the top of circular bar on $\partial\Omega_1$ in [N m]
M^{exact}_{Tmp}	stiffness-based torque on the top of circular bar on $\partial\Omega_1$ in [N m]
M_1, M_2, M_3	external concentrated moment vector in [N m]
m_1, m_2, m_3	external uniform moment vector in [N m]
M_{T}	total torque on the top of circular bar on $\partial\ \Omega_1$ in [N m]
n	unit outward vector normal to the surface in [–]
P_1, P_2, P_3	external concentrated force vector in [N]
p_1, p_2, p_3	external uniform force vector in [N]
$Q^{(n)}$	surface couple in [N m/m^2 or Pa m]
r	position vector in [m]
$t^{(n)}$	surface traction in [Pa]
$r \times \Delta F$	moment provided by position vector r and ΔF in [N m]
$r \times t^{(n)}$	surface couple induced by surface traction in [N m/m^2 or Pa m]
u	displacement vector in [m]

micro-rotations. We have also found a missing part of Cosserat formulation (5) under weak form or so-called virtual work framework whose application substantiates the presence of m_{33} on the top of Cosserat circular bar (Fig. 2), whereas we did not apply any couple traction on the surface for the torsion tests:

$$M_{\mathrm{T}} := M^{exact}_{\mathrm{Tmp}} + M^{exact}_{\mathrm{Tcurv}}. \tag{1}$$

This sustains some moments on the top of specimen under pure torsion test. The achieved numerical experiments give us some ideas about the intrinsic features of Cosserat theory. Indeed, the L_c values cannot be directly link to the micro-structure size or pore size for geo-materials. It handles the relative curvature rigidity comparing to the stiffness rigidity. For the concrete case, L_c parameter is generally defined as a minimum possible homogeneous region through heterogeneous media. This avoids the strain localization instabilities phenomenon during strain softening behavior [6,7]. The Cosserat model has been widely applied to regularize these kinds of problems for the heterogeneous materials, e.g. sand, soil and high porous rocks. This has been achieved by Vardoulakis and co-workers [8], de Borst and co-workers [9,10], Bardet and Proubet [11], Iordache and William [12], Bauer [13], Tejchman and Gudehus [14], Manzari [15], Maier [16] and more recently by Alsaleh and co-workers [17], Riahi and Curran [18], Riahi and co-workers [19] and Jeong and Ramézani [20]. The evaluation of material parameters in Cosserat theory, the analysis of simple shear problem in Cosserat theory, and an enriched Cosserat FEM model can be also addressed in [21–23]. Hence, very large L_c value means that we have a very small specimen or the specimen dimension is less than grid framework or so-called sub-grid state. Very small L_c value signifies that we have a very large specimen, so there is no size effects either. The intermediate zone (zone II) is the most interesting state in which size effect occurs (Fig. 8(a)–(c)). This interpretation would transform the Cosserat theory to an explicit multi-scale tool like those done using micromorphic approach [24,25] and even using multi-length scale assumption [26]. Therefore, we can take into account three different scales, e.g. macro, meso and micro. In this case, we can consider the force equilibrium equation (18a) which prepares the macro-scale stresses and macro-displacements and moment of momentum equilibrium (18b) which provides the micro-scale couple stresses. In this case, we can separately consider the torques for our pure torsion test. Therefore, it is quite reasonable to call the stiffness torque as macro-torque and curvature stiffness torque as micro-torque, respectively. Moreover, their summation will not have a sense either. By assuming the Cosserat theory as an explicit multi-scale approach, we distinguish that it is necessary to achieve the material characterization in macro-scale and micro-scale as well. Hence, the major attempts should be focused on the micro-structural material characterization by means of the modern tools, e.g. nano-indentation for cement paste materials.

1.2. The development of Cosserat models, motivation and applications: An historical overview

This article addresses general continuum models involving independent rotations, which were introduced by the Cosserat's brothers at the beginning of the last century. The basic idea of the Cosserat theory has been proposed by Eugène and François Cosserat in their landmark publication in 1908 [27]. Their original nonlinear and geometrically exact development has been widely forgotten for decades to be only rediscovered by Günther [28], Mindlin and Tiersten [29], Mindlin [30] and Eringen and Suhubi [31], Eringen [32] in a restricted linearized setting in the early sixties. Since then, the original Cosserat concept has been generalized in various directions, notably by Eringen and his coworkers who extended the Cosserat concept to include also micro-inertia effects called micromorphic theory [33,34].[2] The Cosserat theory has been also developed in the fluid mechanics branch [32] and some fresh studies are available in the open literature [38]. The further simplified micropolar theory can be obtained assuming that the macro-rotations are not independent rotations, i.e., they can be related to the displacements, which is named couple stress theory [29,39,40] or so-called "indeterminate couple stress".

The Cosserat theory has been also applied to the human bone [41,42] in the biomechanics branch, foams [43–45] (Lakes' benchmark papers) for the man-made materials or so-called synthetic materials, cellular solids [46] and composites [47]. Some particular applications can be addressed to the metallic foams for energy saving purposes and Voronoi cells [48,49]. Some quite related and outstanding works have been given by Zhang et al. [50] and Providas and Kattis [51] focusing on the analysis of Cosserat materials for contact analysis using 2D-solid and analysis of the structures using 3D-shell elements, respectively. Forest et al. made benchmark contributions in the incremental analysis, finite deformation, strain gradient theory and homogenization aspects for the polycrystalline materials [52–54]. There are also some studies pertaining to the elasto-plasticity of the Cosserat-based media, e.g. Ristinmaa et al. for the couple stress plasticity [55] and Neff and Münch [56] and Jeong–Ramézani [20] based on an original Cosserat concept (geometrically exact Cosserat or non-linear Cosserat).[3]

The infinitesimal and finite elastic–plastic Cosserat theory have been fully investigated [65,20]. It is helpful to mention that the most generalized case, i.e., micromorphic case is also treated and some analytical and 2D numerical analyses are available in the open literature [66,24].

Regardless of kind of materials, most of the available studies have been carried out under 2D-FEM considerations, e.g., [11,67]. This assumption removes some interesting features of Cosserat. Nevertheless, it is usually helpful to get rid of two additional Cosserat material constants comparing to 3D cases. Consequently, it is needed to obtain only one micro-rotation. We turn back and talk about it later in the next sections. Unfortunately, the direct measurements of micro-rotations of particles are not achievable with high accuracy but we can measure the micro-rotation in the diagonal fracture plane by means of the *stereophotometric* method [68].[4]

Over the years, a variety of boundary value problems have been analytically solved which are then used for the determination of material moduli in the infinitesimal linear Cosserat model [71]. Notably, the solution of the pure torsion problem with prescribed torque at the end faces has been given by Gauthier [72,73] and used for the determination of the length scales of different materials. Other attempts have been done by taking advantage of the energy minimization between homogenized Cauchy and Cosserat media. Despite the huge effort spent in investigating the Cosserat model, two main drawbacks still controversially remain. These two points are: the problem of physical meaningful boundary or side-condition for the *micro-rotation* and physically consistent determination of the Cosserat parameters. Our goal is to establish the physical meaningful Cosserat moduli and boundary conditions for Cosserat theory.

1.3. Paper organization

In the present work, we concentrate solely on the Cosserat-based materials using solid mechanics point of view. The determination of the Cosserat parameters micropolar theory, notably case 4 ($\alpha = \beta = \gamma$) is focused on the present work. Furthermore, the most realistic boundary conditions for the micro-rotations involving the grid framework analogy [1,2] are applied into the numerical computations. It is numerically substantiated that the case 4 as like as other cases (case 1, case 2 and conformal case 3) is bounded [4] and the size effects are still revealed.

Our contribution is organized as following: First, we present the linearized Cosserat or so called micropolar mathematical model (*the virtual work approach has been redeemed carefully in order to better understand true coupled nature of Cosserat theory*). We discover a forgotten term or so called *missing term* which represents the coupling between the surface traction and couple traction.[5] Second, we focus on the problem of torsion test of the isotropic brittle material with different cases (cases 1–4). Moreover, the numerical results of Cosserat theory will be compared to the classical continuum media with the identical

[2] Some of Eringen's notations have been revised and corrected later on by Cowin [35] and by Eringen himself [36,37]. The original notations make some flaws and it should be carefully taken into account by the relevant Cosserat moduli or Cosserat material constants.

[3] It is well worth mentioning that the geometrically exact Cosserat non-linear has been recently investigated and some new natural Lagrangian definitions have been proposed in the open literature [57,58] based on Altman's work [59] and Atluri–Cazzani's study [60]. The authors have taken into account these kinematical relations in providing a very robust and highly parallel non-linear 3D-FEM Cosserat models [20]. Some relevant works pertaining to the non-linear Cosserat can be also addressed in [56,58,61–64].

[4] Some benchmark experimental efforts have been made by Lakes [43,44,69,45] for extracting the material unknowns (four supplementary material parameters, i.e., μ_c, α, β and γ). His landmark experiments are still the main experimental reference in the Cosserat society, particularly for the foams. However, his proposed experimental test is not easy to achieve [70].

[5] It can be easily extended to the virtual power approach for the incremental analysis purposes.

loading, geometry and mechanical properties. Some conclusions and outlooks have been provided at the end of the present work whose applications make the Cosserat theory as an explicit multi-scale tool [74]. This equally provides some fresh departures in extracting the Cosserat moduli based upon the subjects, which are discussed in the current study. The last matter probably creates some experimental procedures by means of nano-technology.

2. Linear elastic cosserat theory: fundamental formulations

2.1. Virtual work framework for Cosserat media

For a linear elastic anisotropic Cosserat solid, a total energy density function $W(\bar{\varepsilon},\bar{k})$ can be expressed as a polynomial in function of $\bar{\varepsilon}$ and $\bar{k}$ based on the expansion power series theory [75–77]:

$$W(\bar{\varepsilon},\bar{k}) = W_{\text{mp}}(\bar{\varepsilon},\bar{k}) + W_{\text{cs}}(\bar{\varepsilon},\bar{k}) + W_{\text{curv}}(\bar{\varepsilon},\bar{k}), \tag{2a}$$

$$W_{\text{mp}}(\bar{\varepsilon},\bar{k}) = W^0_{\text{mp}} + \mathbf{S}:\bar{\varepsilon} + \frac{1}{2}\bar{\varepsilon}:\mathbf{D}:\bar{\varepsilon}, \tag{2b}$$

$$W_{\text{cs}}(\bar{\varepsilon},\bar{k}) = W^0{}_{\text{cs}} + \frac{1}{2}\bar{\varepsilon}:\mathbf{C}:\bar{k} + \frac{1}{2}\bar{k}:\mathbf{C}:\bar{\varepsilon} = W^0_{\text{cs}} + \bar{\varepsilon}:\mathbf{C}:\bar{k} \quad \text{where} \quad \bar{\varepsilon}:\mathbf{C}:\bar{k} = \bar{k}:\mathbf{C}:\bar{\varepsilon}, \tag{2c}$$

$$W_{\text{curv}}(\bar{\varepsilon},\bar{k}) = W^0_{\text{curv}} + \mathbf{B}:\bar{k} + \frac{1}{2}\bar{k}:\mathbf{E}:\bar{k}, \tag{2d}$$

where $\bar{\varepsilon}$ is the infinitesimal non-symmetric first Cosserat stretch tensor ($\bar{\varepsilon} = (\nabla u)^T + \overline{A} = (u_{j,i} - e_{ijk}\phi_k)\hat{e}_i \otimes \hat{e}_j$, where, $\nabla u := (\nabla \otimes u)^T = u_{i,j}\hat{e}_i \otimes \hat{e}_j$ and $\overline{A} := \text{anti}\phi = -e\cdot\phi = -e_{ijk}\phi_k\hat{e}_i \otimes \hat{e}_j$). [6]

$\bar{k}$ is the micropolar curvature tensor or wryness tensor ($\bar{k} := \nabla\phi$, where $\nabla\phi := (\nabla \otimes \phi)^T = \phi_{i,j}\hat{e}_i \otimes \hat{e}_j$). In the absence of initial energy densities, stress and couple stress ($W^0_{\text{mp}} = W^0_{\text{cs}} = W^0_{\text{curv}} = 0$ and $\mathbf{S} = \mathbf{B} = \mathbf{0}$) and the hypothesis of centrosymmetry effects for the Cosserat media ($\mathbf{C} = \mathbf{0}$), we can find the following constitutive equations:

$$\bar{\sigma} = \frac{\partial W(\bar{\varepsilon},\bar{k})}{\partial \bar{\varepsilon}} = \mathbf{D}:\bar{\varepsilon}, \tag{4a}$$

$$m = \frac{\partial W(\bar{\varepsilon},\bar{k})}{\partial \bar{k}} = \mathbf{E}:\bar{k}, \tag{4b}$$

where, the fourth order stiffness tensors $\mathbf{D} := D_{ijkl}\hat{e}_i \otimes \hat{e}_j \otimes \hat{e}_k \otimes \hat{e}_l$ and $\mathbf{E} := E_{ijkl}\hat{e}_i \otimes \hat{e}_j \otimes \hat{e}_k \otimes \hat{e}_l$ deal with the stiffness and curvature stiffness of the material, respectively.

According to the virtual work principle (Fig. 1), the relation between the virtual elastic strain energy density and the potential energy function on the body having volume Ω and surface $\partial\Omega$ in the case of the Cosserat framework can be derived as below [76,78]:

$$\int_\Omega \bar{\sigma}^T:\delta\bar{\varepsilon}\,dV + \int_\Omega m^T:\delta\bar{k}\,dV = \int_{\partial\Omega_t} t^{(n)}\cdot\delta u\,dS + \int_\Omega \rho b\cdot\delta u\,dV + \int_{\partial\Omega_c} Q^{(n)}\cdot\delta\phi\,dS + \int_{\partial\Omega_t}(r\times t^{(n)})\cdot\delta\phi\,dS + \int_\Omega \rho c\cdot\delta\phi\,dV, \tag{5}$$

where, $t^{(n)}$ and $\overline{Q}^{(n)}$ are the surface traction and total surface couple, respectively:

$$\bar{\sigma}^T\cdot n = t^{(n)} \quad or \quad \bar{\sigma}_{ji}n_j = t^{(n)}_i \quad \text{for} \quad i,j = 1,2,3 \tag{6a}$$

and

$$m^T\cdot n = \overline{Q}^{(n)} \quad \text{or} \quad m_{ji}n_j = \overline{Q}^{(n)}_i \quad \text{for} \quad i,j = 1,2,3 \quad \text{where} \quad \overline{Q}^{(n)} = Q^{(n)} + r\times t^{(n)}, \tag{6b}$$

where, n is the unit outward vector normal to the surface S. In (5), we have an additional term at the right hand side $\left(\int_{\partial\Omega_t}(r\times t^{(n)})\cdot\delta\phi\,dS\right)$. This *missing term* represents the impact of the applied surface traction on the couple traction and it plays an important role in the coupling.

Let's take (5), the integration over $\partial\Omega_t$ can be replaced by $\partial\Omega$ due to the fact that $\delta u_i = 0$ on $\partial\Omega_u$ and $t^{(n)}_{ij} = 0$ on $\partial\Omega_0 \cup \partial\Omega_c$. The integration over $\partial\Omega_c$ can be similarly substituted by $\partial\Omega$ due to the fact that $\delta\phi_i = 0$ on $\partial\Omega_u$ and

[6] The Cosserat first stretch tensor composes the symmetrical ($\text{sym}\,\bar{\varepsilon} = \text{sym}\,\nabla u = \frac{1}{2}(u_{j,i} + u_{i,j})\hat{e}_i \otimes \hat{e}_j$) and antisymmetrical ($\text{skew}\bar{\varepsilon} = \text{skew}\nabla u - \mathbf{e}\cdot\phi = (\frac{1}{2}(u_{j,i} - u_{i,j}) - e_{ijk}\phi_k)\hat{e}_i \otimes \hat{e}_j$) counterparts:

$$\bar{\varepsilon} = \text{sym}\,\bar{\varepsilon} + \text{skew}\bar{\varepsilon} = (\nabla u)^T + \overline{A} = (\nabla u)^T - e\cdot\phi = (u_{j,i} - e_{ijk}\phi_k)\hat{e}_i \otimes \hat{e}_j \quad \text{for} \quad i,j = 1,2,3. \tag{3}$$

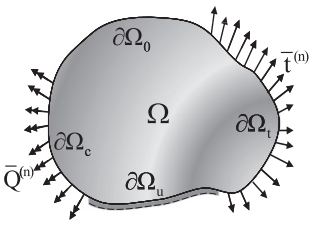

Fig. 1. Typical illustration of a solid body subjected to surface traction and surface couple.

$Q_{ij}^{(n)} = 0$ on $\partial\ \Omega_0 \cup \partial\Omega_t$. We use also the same procedure for $\int_{\partial\Omega_t}(r \times t^{(n)}) \cdot \delta\phi\, dS$ by considering $\delta\phi_i = 0$ on $\partial\Omega_u$ and $r \times t^{(n)} = 0$ on $\partial\Omega_0 \cup \partial\Omega_c$:

$$\int_\Omega \bar{\sigma}^T : \delta\bar{\varepsilon}\, dV + \int_\Omega m^T : \delta\bar{k} dV = \int_{\partial\Omega} t^{(n)} \cdot \delta u\, dS + \int_\Omega \rho b \cdot \delta u\, dV + \int_{\partial\Omega} Q^{(n)} \cdot \delta\phi\, dS + \int_{\partial\Omega} (r \times t^{(n)}) \cdot \delta\phi\, dS + \int_\Omega \rho c \cdot \delta\phi\, dV, \tag{7}$$

or

$$\int_\Omega \bar{\sigma}^T : \delta\bar{\varepsilon}\, dV + \int_\Omega m^T : \delta\bar{k} dV = \int_{\partial\Omega} t^{(n)} \cdot \delta u\, dS + \int_\Omega \rho b \cdot \delta u\, dV + \int_{\partial\Omega} \overbrace{(Q^{(n)} + (r \times t^{(n)}))}^{\bar{Q}^{(n)} := Q^{(n)} + r \times t^{(n)}} \cdot \delta\phi\, dS + \int_\Omega \rho c \cdot \delta\phi\, dV \tag{8}$$

By applying divergence theorem and some absolute notation operations, the following relations could be inferred (see Appendix (A)):

$$\int_{\partial\Omega} t^{(n)} \cdot \delta u\, dS = \int_\Omega (\mathrm{Div}\,\bar{\sigma} \cdot \delta u + \bar{\sigma}^T : \nabla\delta u)\, dV, \tag{9a}$$

$$\int_{\partial\Omega} \bar{Q}^{(n)} \cdot \delta\phi\, dS = \int_\Omega (\mathrm{Div}\, m \cdot \delta\phi + m^T : \nabla\delta\phi)\, dV. \tag{9b}$$

The term $\int_\Omega \bar{\sigma}^T : \delta\bar{\varepsilon}\, dV$ can be denoted in function of ∇u and ϕ using $\delta u_{i,j} = \delta u_{j,i}$ as:

$$\int_\Omega \bar{\sigma}^T : \delta\bar{\varepsilon}\, dV = \int_\Omega \bar{\sigma}^T : \delta((\nabla u)^T - e \cdot \phi)\, dV = \int_\Omega \bar{\sigma}^T : (\delta(\nabla u)^T - e \cdot \delta\phi)\, dV = \int_\Omega (\bar{\sigma}^T : \delta\nabla u - \bar{\sigma}^T : (e \cdot \delta\phi))\, dV. \tag{10}$$

We can easily verify that $\bar{\sigma}^T : (e \cdot \delta\phi) = (e \cdot \delta\phi) : \bar{\sigma}^T = -(e : \bar{\sigma}) \cdot \delta\phi$, so, $\int_\Omega \bar{\sigma}^T : \delta\bar{\varepsilon}\, dV$ can be further simplified as below:

$$\int_\Omega \bar{\sigma}^T : \delta\bar{\varepsilon}\, dV = \int_\Omega (\bar{\sigma}^T : \nabla\delta u + (e : \bar{\sigma}) \cdot \delta\phi)\, dV. \tag{11}$$

Another term or curvature virtual work $\left(\int_\Omega m^T : \delta\bar{k}\right)$ is written:

$$\int_\Omega m^T : \delta\bar{k} dV = \int_\Omega m^T : \delta\nabla\phi\, dV = \int_\Omega m^T : \nabla\delta\phi\, dV. \tag{12}$$

By substituting (9a), (9b), (11) and (12) into (8), we extract the following equation:

$$\begin{aligned} &\int_\Omega \left(\bar{\sigma}^T : \nabla\delta u + (e : \bar{\sigma}) \cdot \delta\phi\right) dV + \int_\Omega m^T : \nabla\delta\phi\, dV \\ &= \int_\Omega (\mathrm{Div}\,\bar{\sigma} \cdot \delta u + \bar{\sigma}^T : \nabla\delta u)\, dV + \int_\Omega \rho b \cdot \delta u\, dV + \int_\Omega (\mathrm{Div}\, m \cdot \delta\phi + m^T : \nabla\delta\phi)\, dV + \int_\Omega \rho c \cdot \delta\phi\, dV. \end{aligned} \tag{13}$$

The above equation would be further simplified and some terms get canceled:

$$\int_\Omega (e : \bar{\sigma}) \cdot \delta\phi\, dV = \int_\Omega \mathrm{Div}\,\bar{\sigma} \cdot \delta u\, dV + \int_\Omega \rho b \cdot \delta u\, dV + \int_\Omega \mathrm{Div}\, m \cdot \delta\phi\, dV + \int_\Omega \rho c \cdot \delta\phi\, dV \tag{14}$$

and, we have got the final weak form:

$$\int_\Omega (\mathrm{Div}\,\bar{\sigma} + \rho b) \cdot \delta u\, dV + \int_\Omega (\mathrm{Div}\, m - e : \bar{\sigma} + \rho c) \cdot \delta\phi\, dV = 0. \tag{15}$$

The concept of virtual work within virtual displacements and micro-rotations leads to the following relations:

$$\mathrm{Div}\,\bar{\sigma} + \rho b = 0 \quad \text{and} \quad \mathrm{Div}\,m - e : \bar{\sigma} + \rho c = 0 \quad \text{in} \quad \Omega, \tag{16a}$$

$$\bar{\sigma}^T \cdot n = t^{(n)} \quad \text{on} \quad \partial\Omega_t \quad \text{and} \quad \bar{\sigma}^T \cdot n = 0 \quad \text{on} \quad \partial\Omega_0 \cup \partial\Omega_c, \tag{16b}$$

$$m^T \cdot n = \overline{Q}^{(n)} = Q^{(n)} + 0 \quad \text{on} \quad \partial\Omega_c, \quad m^T \cdot n = \overline{Q}^{(n)} = 0 + 0 \quad \text{on} \quad \partial\Omega_0 \tag{16c}$$

and

$$m^T \cdot n = \overline{Q}^{(n)} = 0 + r \times t^{(n)} \quad \text{on} \quad \partial\Omega_t. \tag{16d}$$

It should be notified that $\overline{Q}^{(n)}$ or so called total couple traction can be defined as below:

$$\overline{Q}^{(n)} = Q^{(n)} + r \times t^{(n)}. \tag{17}$$

The term $r \times t^{(n)}$ deals with the additional couple traction due to the presence of surface traction $t^{(n)}$.

According to the above-mentioned procedure, the *total couple traction* $\overline{Q}^{(n)}$ contains *well-known couple traction vector* and *the impact of surface traction*. Hence, for pure torsion test, though we did not apply any couple traction, the total couple traction does not vanish due to the presence of Dirichlet boundary conditions using exact angle (Fig. 2).

We show later on the effect of this term in calculating of torsion tests via m_{33}.

As pointed out before, the presence of the surface traction induces some surface couples. This principle can be equally extended into the micromorphic medium.[7] In the absence of macro, micro-accelerations, body force and body couple, the equilibrium equations of the Cosserat theory are given as:

$$\mathrm{Div}\,\bar{\sigma} = 0 \quad \text{or} \quad \bar{\sigma}_{ji,j} = 0 \quad \text{for} \quad i,j = 1,2,3, \tag{18a}$$

$$\mathrm{Div}\,m - e : \bar{\sigma} = 0 \quad \text{or} \quad m_{ji,j} - e_{ijk}\bar{\sigma}_{jk} = 0 \quad \text{for} \quad i,j = 1,2,3. \tag{18b}$$

(18a) and (18b) imply that stress tensor $\bar{\sigma}_{ij}$ is not necessarily symmetric and its antisymmetrical part is determined by the divergence of the couple stress tensor m_{ij}. In order to quantify the nature of the internal distribution of forces and moments within a continuum solid, a general body subject to arbitrary (concentrated and distributed) external loadings is considered (Fig. 3).

To investigate the internal forces, a section is made through the body as shown. On this section consider an infinitesimal area ΔA with outward unit normal vector n. The resultant surface force and surface couple acting on ΔA is defined by ΔF and ΔM. As illustrated in Fig. 3, the surface traction, surface couple and total surface couple are defined. As illustrated in Fig. 3, the presence of ΔF creates an $r \times \Delta F$ that it yields $r \times t^{(n)}$. Assuming isotropy properties, the fourth order stiffness tensors in the constitutive equations, (4a) and (4b) can be rewritten and simplified as below:

$$\bar{\sigma} = 2\mu\ \mathrm{sym}\,\bar{\varepsilon} + 2\mu_c \mathrm{skew}\bar{\varepsilon} + \lambda\ \mathrm{tr}\ [\bar{\varepsilon}]\mathbb{I} \quad \text{or} \quad \bar{\sigma} = (\mu + \mu_c)\bar{\varepsilon} + (\mu - \mu_c)\bar{\varepsilon}^T + \lambda \mathrm{tr}[\bar{\varepsilon}]\mathbb{I} \tag{19}$$

and

$$m = \beta\bar{k} + \gamma\bar{k}^T + \alpha \mathrm{tr}[\bar{k}]\mathbb{I} = \beta\nabla\phi + \gamma\nabla\phi^T + \alpha \mathrm{tr}[\nabla\phi]\mathbb{I}, \tag{20a}$$

or

$$m = (\gamma + \beta)\mathrm{dev}\,\mathrm{sym}\,\nabla\phi + (\gamma - \beta)\ \mathrm{skew}\nabla\phi + \frac{3\alpha + (\beta + \gamma)}{2}\mathrm{tr}[\nabla\phi]\mathbb{I} \tag{20b}$$

λ and μ, are the classical Lamé's constants and μ_c, α, β and γ are new additional material parameters introduced into Cosserat theory. The classical macro-rotations $\bar{\omega}$ can be described as below:

$$\bar{\omega} := \mathrm{axl}(\mathrm{skew}\nabla u) = \frac{1}{2}\nabla \times u \quad \text{or} \quad \bar{\omega} := -\frac{1}{2}\mathbf{e} : \omega = -\frac{1}{2}e_{ijk}\omega_{jk}\hat{e}_i \quad \text{where} \quad \omega := \mathrm{skew}\nabla u = \frac{1}{2}(u_{i,j} - u_{j,i})\hat{e}_i \otimes \hat{e}_j \tag{21}$$

It is assumed that the micro-rotation vector field (micro-rotation or micro-rotation) is kinematically independent from the displacement vector field, u and macro-rotation, $\bar{\omega}$. In the Cosserat continuum theory not only forces but also moments can be transmitted across the surface of a material element. The concept of Cosserat theory involves the micro-structures into the continuum media by the micro-rotation effect (Fig. 4).

In the next section, we focus on case 4 and some physical meaningful boundary conditions or side-conditions for the independent micro-rotations.

2.2. Evaluation of the material parameters in Cosserat theory and micro-rotation boundary conditions

In this section, we attempt to handle two salient problems of the Cosserat-based continuum, i.e. material parameters determination and physically meaningful boundary conditions for the micro-rotations. Let us take the first subject. According to (19) and (20a), it is easy to conclude that when, μ_c, α, β and γ vanish, the solid becomes classically elastic. By taking

[7] The micromorphic continuum is out of scope of this paper and it is needed to be considered as a whole by another study.

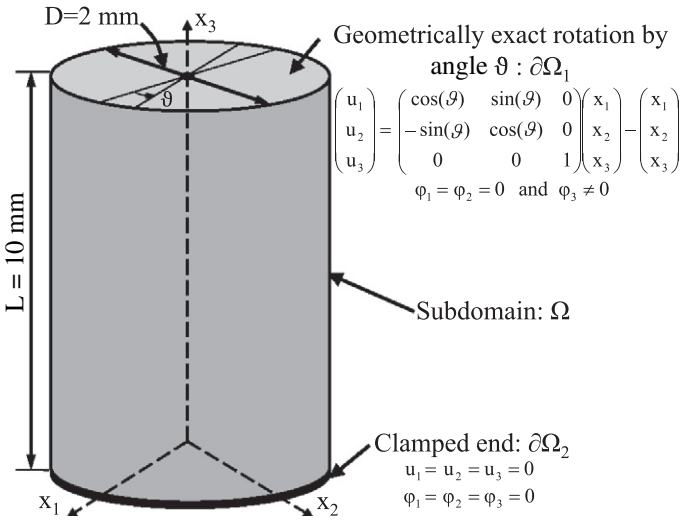

Fig. 2. Torsion test geometry and boundary conditions.

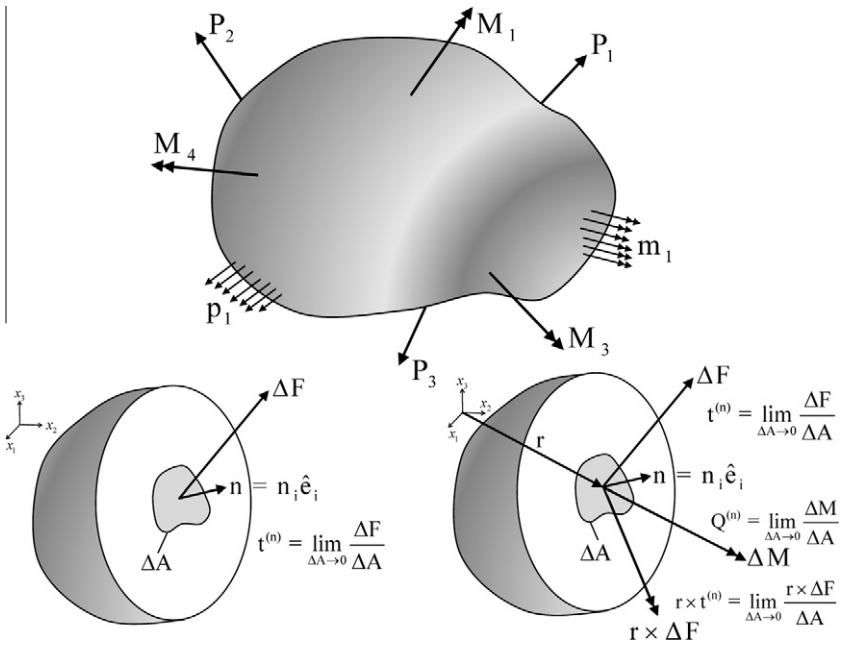

Fig. 3. Typical presentation of surface and couple traction for a solid body subjected to arbitrary external loadings, top: Externally loaded body, bottom-left: Sectioned body for Cauchy–Boltzmann's media (Description of the surface traction $t^{(n)}$ vector on a sectioned area), bottom right: Sectioned body for micropolar media (Description of the surface couple $Q^{(n)}$ and $r \times t^{(n)}$ vectors on a sectioned area (r is the position vector)).

advantage of the mathematical points of view, the strain energy density $W_{\mathrm{mp}}(\bar{\varepsilon}, \bar{k})$ and the curvature energy density $W_{\mathrm{curv}}(\bar{\varepsilon}, \bar{k})$ would have the local positivity condition. But that is not sufficed and the positive definiteness of stiffness of constitutive laws would be also required (see. Appendix B) [3]:

$$\mu \geqslant 0, \quad ,3\lambda + 2\mu \geqslant 0 \quad ,\mu_c \geqslant 0, \quad \beta + \gamma \geqslant 0 \quad ,3\alpha + (\beta + \gamma) \geqslant 0 \quad ,\gamma - \beta \geqslant 0 \quad ,\gamma \geqslant 0. \tag{22}$$

Traditionally, the four supplementary material parameters, i.e., μ_c, α, β and γ can be expressed by the other terms, ℓ_b, ℓ_t, N, Ψ [43,70,80]. They represent the characteristic length scale for bending, characteristic length scale for torsion, coupling number and polar ratio, respectively.

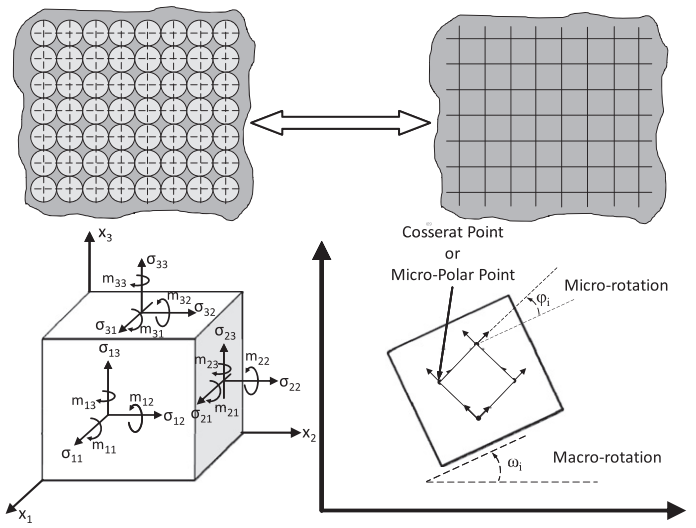

Fig. 4. Top: Modeling of heterogeneous materials with microstructure, bottom left: Components of stress and couple stress tensors for micropolar solids, bottom right: Micro-rotation comparing to the macro-rotation [79].

The above-defined so-called material parameters have been substantially applied for determining the Cosserat material constants, notably by Lakes. The previously indicated Cosserat moduli (μ_c, α, β and γ) could be denoted as below [77]:[8]

$$\ell_b^2 := \frac{\gamma}{2(2\mu^* + \kappa)} \quad \text{and} \quad \ell_t^2 := \frac{\beta + \gamma}{2\mu^* + \kappa}, \tag{23a}$$

$$N^2 := \frac{\mu_c}{\mu + \mu_c} = \frac{\kappa}{2(\mu^* + \kappa)} \quad \text{where} \quad 0 \leqslant N^2 \leqslant 1, \tag{23b}$$

$$\Psi := \frac{\beta + \gamma}{\alpha + \beta + \gamma} \quad \text{where} \quad 0 \leqslant \Psi \leqslant \frac{3}{2}, \tag{23c}$$

where, κ and μ^* are the Cosserat couple modulus and Pseudo-Lamé's constant in accordance with the Eringen's notation. If μ_c tends to infinity, the Cosserat media becomes the couple stress theory or so-called indeterminate couple stress theory and then the coupling number becomes one ($N = 1$) [29,39,40]. The indeterminate couple stress case could be also found out for very large values of L_c via the analytical and numerical methods [4,5]. According to the thermodynamical and mathematical considerations the polar ratio cannot exceed the value of $\frac{3}{2}$ [37,43,77].

Let us take into account two relevant constitutive laws of the Cosserat theory (19) and (20a). As pointed out before, there are two distinct sets of parameters: (λ, μ and μ_c) which relate the traditional stresses and strains and have a dimension of force per unit area ([Pa]), and (α, β and γ) which relate to the higher-order couple stresses to micropolar curvature tensor, with a dimension of force ([N]). Due to the dimensional difference between the two sets of parameters, at least three intrinsic characteristic lengths can be then defined for an isotropic elastic Cosserat material. These characteristic length scales can be generalized based upon the studies which have done earlier [39,81,47] as below:

$$\ell_1^2 := \frac{\alpha}{\mu}, \quad \ell_2^2 := \frac{\beta}{\mu} \quad \text{and} \quad \ell_3^2 := \frac{\gamma}{\mu}, \tag{24}$$

where, ℓ_1, ℓ_2 and ℓ_3 are new characteristic length scales corresponding to the trace counterpart of micropolar curvature tensor ($\mathrm{tr}[\bar{k}]$), curvature tensor itself ($\bar{k}$) and its transposed ($\bar{k}^T$), respectively. As indicated before, six Cosserat parameters should be taken into account for 3D isotropic Cosserat elasticity, i.e. $(\lambda, \mu, \mu_c, \alpha, \beta, \gamma) \mapsto (\lambda, \mu, \mu_c, \ell_1, \ell_2, \ell_3)$. Using the definition of Ψ and (24), the polar ratio and coupling number can be inferred as:

$$\Psi = \frac{\beta + \gamma}{\alpha + \beta + \gamma} = \frac{\ell_2^2 + \ell_3^2}{\ell_1^2 + \ell_2^2 + \ell_3^2} \quad \text{and} \quad N^2 = \frac{\mu_c}{\mu + \mu_c}. \tag{25}$$

[8] To avoid any conflict among the available Cosserat moduli, we use the state-of-the-art formulations [4,5,77] which contain some corrections provided by Cowin [35].

If three characteristic length scales become identical, this violates the positive definiteness of curvature energy density as well as lack of control on skew symmetric counterpart of the curvature energy density (see Appendix C):[9]

$$W_{\text{curv}}(\bar{\varepsilon},\bar{k}) = \frac{1}{2}(\alpha \text{tr}[\bar{k}]^2 + (\beta+\gamma)\text{sym}\,\bar{k} : \text{sym}\,\bar{k} + (\gamma-\beta)\text{skew}\bar{k} : \text{skew}\bar{k}), \tag{29a}$$

or

$$W_{\text{curv}}(\bar{\varepsilon},\bar{k}) = \frac{1}{2}\left(\alpha \bar{k}_{ii}\bar{k}_{jj} + (\beta+\gamma)\bar{k}_{ij}^{\text{sym}}\bar{k}_{ij}^{\text{sym}} + (\beta-\gamma)\bar{k}_{ij}^{\text{skew}}\bar{k}_{ij}^{\text{skew}}\right), \tag{29b}$$

where $\bar{k}_{ij}^{\text{sym}}$ and $\bar{k}_{ij}^{\text{skew}}$ are symmetric and skew symmetric parts of the micropolar curvature tensor, respectively.

The positive definiteness of the second constitutive law (couple stress-micropolar curvature relation) is traditionally important in the classical solid mechanics. Nevertheless, the main question is that "*Is it necessary to take this strong condition on every constitutive law or not*?". In the classical theory of continuum mechanics, we require to satisfy two conditions: first condition is positive definiteness of the constitutive law and second is the local positivity of strain energy density. The local positivity of strain energy density is automatically fulfilled by the fact that there is linear elasticity property (The linear elasticity property provides a quadratic form of strain energy density and it is always local positive). But, in the Cosserat-based continuum media, we have two constitutive laws and two kinds of energy density excluding the centrosymmetrical energy density, i.e., strain energy density and curvature energy density. So, it is quite possible to have the local positivity of total energy density (the sum of strain energy density, $W_{\text{mp}}(\bar{\varepsilon},\bar{k})$ and curvature strain energy, $W_{\text{curv}}(\bar{\varepsilon},\bar{k})$ is positive, i.e. $W(\bar{\varepsilon},\bar{k}) := W_{\text{mp}}(\bar{\varepsilon},\bar{k}) + W_{\text{curv}}(\bar{\varepsilon},\bar{k}) > 0$) when one constitutive law between the available constitutive laws becomes semi-positive definite. This case is the weakest possible case in which the problem is still *well-posed*. The above-mentioned case has been analytically investigated by Neff and Jeong in [3]. We have numerically investigated it in the following numerical models. From recent analytical investigations, the following classification has been extracted:

- Case (1) $\alpha = \beta = 0$ and $\gamma = \mu L_c^2$ [82,5,83],

$$W_{\text{curv}} := \frac{\mu L_c^2}{2}(\nabla\phi : \nabla\phi) = \frac{\mu L_c^2}{2}\|\nabla\phi\|^2 \tag{30}$$

- Case (2) $\alpha = 0$ and $\beta = \gamma = \frac{1}{2}\mu L_c^2$ [4,5],

$$W_{\text{curv}} := \frac{\mu L_c^2}{2}(\text{sym}\,\nabla\phi : \text{sym}\,\nabla\phi) = \frac{\mu L_c^2}{2}\|\text{sym}\,\nabla\phi\|^2 \tag{31}$$

- Case (3) $\alpha = -\frac{1}{3}\mu L_c^2$ and $\beta = \gamma = \frac{1}{2}\mu L_c^2$ [3–5,84–86],

$$\begin{aligned} W_{\text{curv}} &:= \frac{\mu L_c^2}{2}(\text{dev}\,\text{sym}\,\nabla\phi : \text{dev}\,\text{sym}\,\nabla\phi) = \frac{\mu L_c^2}{2}(\text{sym}\,\nabla\phi : \text{sym}\,\nabla\phi - \frac{1}{3}\text{tr}[\nabla\phi]^2) \\ &= \frac{\mu L_c^2}{2}(\|\text{sym}\,\nabla\phi\|^2 - \frac{1}{3}\ \text{tr}[\nabla\phi]^2). \end{aligned} \tag{32}$$

- Case (4) $\alpha = \beta = \gamma = \mu L_c^2$ [20].

$$\begin{aligned} W_{\text{curv}} &:= \frac{\mu L_c^2}{2}(\nabla\phi : \nabla\phi + \nabla\phi^T : \nabla\phi + \text{tr}[\nabla\phi]^2) = \frac{\mu L_c^2}{2}(\|\nabla\phi\|^2 + \nabla\phi^T : \nabla\phi + \ \text{tr}[\nabla\phi]^2) \\ &= \frac{\mu L_c^2}{2}(\|\nabla\phi\|^2 + \ \text{tr}[(\nabla\phi)^2] + \text{tr}[\nabla\phi]^2). \end{aligned} \tag{33}$$

All cases apart from "case 1" reveal the independency properties. Hence, the recently developed relations (cases 2–4) not only remove the well-known problem of dependency but also they reduce the Cosserat moduli to only four (λ, μ, μ_c and L_c) for the 3D-FEM models. The aforementioned hypothesis about the equality of the Cosserat models covers neatly the Cosserat redundant material constants and independency drawback dilemmas and probably gives one physical meaningful idea about the characteristic length scales. It also satisfies the required conditions for bending and torsion [77]. In the next section, we take advantage of the shown Cosserat moduli and we trigger to analyze some familiar loadings particularly, *pure torsion*.

[9] The symmetric and skew symmetric part of the micropolar curvature density can be defined as below:

$$\bar{k} := \text{sym}\,\bar{k} + \text{skew}\bar{k} = \bar{k}_{ij}^{\text{sym}}\hat{e}_i\otimes\hat{e}_j + \bar{k}_{ij}^{\text{skew}}\hat{e}_i\otimes\hat{e}_j, \tag{26}$$

where

$$\text{sym}\,\bar{k} := \bar{k}_{ij}^{\text{sym}}\hat{e}_i\otimes\hat{e}_j = \frac{1}{2}(\bar{k}_{ij}+\bar{k}_{ji})\hat{e}_i\otimes\hat{e}_j, \tag{27}$$

$$\text{skew}\bar{k} := \bar{k}_{ij}^{\text{skew}}\hat{e}_i\otimes\hat{e}_j = \frac{1}{2}(\bar{k}_{ij}-\bar{k}_{ji})\hat{e}_i\otimes\hat{e}_j. \tag{28}$$

2.3. Physically meaningful micro-rotation boundary conditions or side-conditions for boundary value problem

In this sub-section, we focus on the physically meaningful micro-rotation boundary conditions. As pointed out before, many analytical solutions have been made for determining the L_c values using the torsion tests [72,73,44]. It is evident that this case provides the most micro-rotations magnitude. Nevertheless, it is *not unique way* to obtain the micro-rotations [87]!

We took into account the beam-based structure or grid frameworks models assumptions (see top of Fig. 4) in [1,2,78]. It is well-known that the micro-rotations would be assimilated as the rotations at the nodes of a beam-based structures. Regardless, whether the loading type is torsional or not, it is quite possible to acquire the rotation vector by taking advantage of grid frameworks model. The major difference is nothing else than the value of this vector!

The above-indicated beam-structure assumption automatically allows us to consider the same boundary conditions for the micro-rotation vector. This issue drastically changes the solution form of a boundary value problem and the convergence problem gets better, particularly for very large L_c values (boundedness property of the Cosserat theory).[10]

It is of great importance to recall that the open literatures try to relax the Dirichlet boundary conditions for micro-rotations and these kinds of boundary conditions are called the artificial boundary conditions.

As a matter of fact, in the Cosserat theory, the stiffness comes from two sources, i.e. the "displacement"-based stiffness or so-called stiffness and the "micro-rotation"-based stiffness or so-called curvature stiffness. The original Cosserat idea links them via micro-rotations but they have their own distinct boundary conditions corresponding to the displacements for solid elements and beam elements, respectively.

Now, we attempt to put into practice these proposed solutions for the salient Cosserat dilemmas. To achieve this goal, we get started with some interesting loadings, specially, pure torsion.

3. 3D-FEM of linear Cosserat elasticity

In this work, we will discuss the finite-element simulation of the linear Cosserat model with the new micropolar constants $\left(\alpha=\beta=\gamma=\mu L_c^2\right)$ in which the above-described drawback does not take place (μ_c and L_c dependency). The finite element analysis of Cosserat materials has been already studied in the literature. Early works on the finite element analysis based on the Cosserat theory are those done by Baluch et al. [88] and Nakamura et al. [89] in which a simple three-node triangle element with three degrees of freedom at each node is used for a two-dimensional problem. A higher-order triangle element again for a two-dimensional analysis based on Cosserat elasticity has been recently proposed by Providas and Kattis [51], and Trovalusci and Masiani [90] treats the 2D-nonlinear case. The Cosserat theory has also been employed by Nadler and Rubin to formulate a three-dimensional finite element for dynamic analysis in nonlinear elasticity [91]. In addition, higher-order elements for elastic analysis of shells have been proposed by Jog [92]. An example calculation of the linear isotropic Cosserat model for two-dimensional finite elements has been performed by Li and Xie [93]. There are also some studies in the literature for foams [94–96]. Huang et al. [97], Zastrau and co-workers [98,99] have done very early attempts based on the Cosserat curvature parameter choice $\alpha=\beta=0,\ \gamma>0$ and $\beta=\gamma>0,\ \alpha\geqslant 0$, respectively.

Though several numerical studies have been done for Cosserat materials only few of them treat the full three-dimensional case [100,62]. The two-dimensional Cosserat setting automatically removes two material parameters and the altogether required Cosserat material moduli reduce to only four (the two-dimensional problem is much simpler because of a fixed axis of rotations). Moreover, the 2D assumptions yield case 1 ($\alpha=\beta=0$ and $\gamma=\mu L_c^2$) in which there is one of the Cosserat dilemmas! Furthermore, the size effect that is explicitly embedded in the Cosserat-based continuum media, does not entirely happen by neglecting the effect of the other dimensions and their interactions. Consequently, we did not provide any numerical experiment pertaining to case 1 throughout this study.

While we have a geometrically exact 3D-code successfully running we present here only the "linear" version for mainly two reasons:[11] first, other groups do not necessarily have access to a 3D-geometrically exact code, making comparison impossible, and second, we investigate a novel situation (case 4) where already the linear response shows interesting features. Moreover, we solely concentrate on fully three-dimensional finite element models. Particularly, we focus on the torsion test of the circular bars.

In the next sub-sections, we are motivated to achieve the 3D numerical experiments including the proposed solutions.

3.1. Linear Cosserat elasticity implementations

The finite element method has been chosen as a relevant numerical method for the linear elastic Cosserat model. All computations are provided by a user-written code within the general purpose FEM software COMSOL MP. We have used

[10] The solution of a boundary value problem radically depends on the applied Dirichlet boundary conditions, whereas the Neumann boundary conditions are not capable of changing the general form of solution.

[11] The non-linear Cosserat simulation has been already handled by Sansour [63] and Münch [62].

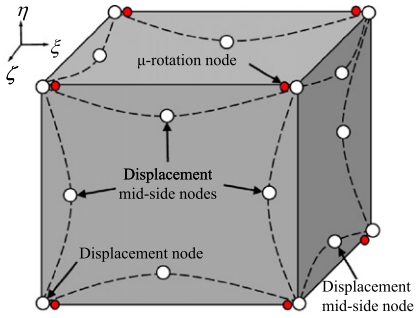

Fig. 5. Presentation of high-order 28-node solid hexahedral element involving 20 nodes for displacements and 8 nodes for micro-rotations.

a parallelized iterative solver making it possible to reduce the computation runtime: here an Intel-System with 32 GB memory and 8 core 3.2 GHz processor has been used. An isotropic linear Cosserat computation with 4.34 Mi DOFs[12] would last 17 min for case 4 including $\mu_c = \mu$ assumption.

We use *iso-parametric Lagrange shape functions* in our study. Moreover, we use *quadratic* Lagrange shape function for the displacement vector u and *linear* Lagrange shape function for the entries of the dual tensor of micro-rotation vector $-\overline{A} \in \mathfrak{so}(3)$ (Fig. 5).

This choice leads to the same order of magnitude for ∇u and ϕ in $\bar{\varepsilon} = (\nabla u)^T + \overline{A} = (u_{j,i} - e_{ijk}\phi_k)\hat{e}_i \otimes \hat{e}_j$ which is very important to find out the mesh-independency feature for the numerical outcomes [62]. As will be seen later, in altogether numerical simulations, the hexagonal solid elements with appropriate mesh density have been utilized.

As illustrated in Fig. 5, the 28-node brick elements are used for the numerical simulation using reduced integration. Consequently, each element prepares 28×3 DOFs, this is why the 3D-FEM analysis of Cosserat-based media is rather expensive in terms of numerical computation. This matter does not end here because the FEM analyses entail also the unsymmetrical solver algorithms and some parallelism issues.

According to the discussed balance equations, there are six available state variables (three for the displacement vector u and three for the micro-rotation vector $\mathrm{axl}\left(\overline{A}\right)$) whose computations need to be done via the coupled linear partial differential system of equations using the momentum and angular momentum balance equations based upon the weak form. It is of importance to note that the Cosserat couple modulus μ_c is assumed to be equal to μ throughout this paper ($\mu_c = \mu$).

3.2. 3D-FEM analysis of torsion test

We consider a cylindrical bar (diameter = 2 mm, height = 10 mm) submitted to the torsion angle ϑ at the end and choose the $\hat{e}_3$-axis to coincide with the axis in Fig. 2. The assumed classical, size-independent parameters E, ν as well as size-dependent parameters can be found in Table 1.

In this subsection, we apply the beam network postulate for micro-rotations as a relevant boundary condition for the curvature stiffness computations as well as the classical boundary conditions for stiffness computations in the followed numerical experiments (Fig. 2). As illustrated in Fig. 2, we apply an exact angle on the top of circular bar and only micro-rotation in x_3 is released by analogy with the beam network or grid frameworks model. The main advantage of the above-mentioned boundary conditions on the top of Cosserat circular bar is that we can apply exact angle of rotation whether it is small or large without any lack of precision (geometrically exact rotation). This entails some computations in conjunction with the deformation gradient tensor $F := \mathbb{I} + \nabla u$, particularly for large rotations.

We would like to be as close as possible to the exact rotation concept. As will be seen later, the grid framework model assumption for micro-rotations provides more convergent models for all cases and the models are completely bounded whatever the value of L_c. By taking advantage of the numerical calculations, we substantiate the presence of so-called missing term $\left(\int_{\partial\Omega_t}(r \times t^{(n)}) \cdot \delta\phi \, dS\right)$ in (5) which could be emphasized by m_{33}. In fact, the value of m_{33} is not negligible for Cosserat circular bar, whereas we did not apply any couple traction ($Q^{(n)}$) on the top of circular bar! In according to the extracted results, both stiffness torque M_{Tmp} or curvature stiffness torque M_{Tcurv} are bounded and the value of the second term is high enough comparing to the first term regarding large and very large L_c values.

3.2.1. Torsion test numerical experiments: mesh density, mesh-independency and convergence issue

As previously explained, the Cosserat theory takes into account automatically the size effect through the additional materials constants, i.e. μ_c, α, β and γ. The main important issue is the mesh-dependency subject. As a matter of fact, the numerical

[12] In all computations through this study, DOFs in conjunction with Lagrange multipliers are accounted for our numerical statistics.

Table 1
Representative material properties for Cosserat circular bar for L_c values between 0 and 1×10^7 mm ($0 \leqslant L_c \leqslant 1 \times 10^7$ mm) including all cases (case 1, case 2, conformal case 3 and case 4).

Cases	E [MPa]	ν [–]	μ [MPa]	λ [MPa]	μ_c [MPa]	α [N]	β [N]	γ [N]	Ψ [–]	N^2 [–]
Case 1	1×10^6	0.3	$\frac{E}{2(1+\nu)}$	$\frac{\nu E}{(1+\nu)(1-2\nu)}$	μ	0	0	μL_c^2	1	$\frac{1}{2}$
Case 2	1×10^6	0.3	$\frac{E}{2(1+\nu)}$	$\frac{\nu E}{(1+\nu)(1-2\nu)}$	μ	0	$\frac{1}{2}\mu L_c^2$	$\frac{1}{2}\mu L_c^2$	1	$\frac{1}{2}$
Case 3	1×10^6	0.3	$\frac{E}{2(1+\nu)}$	$\frac{\nu E}{(1+\nu)(1-2\nu)}$	μ	$-\frac{1}{3}\mu L_c^2$	$\frac{1}{2}\mu L_c^2$	$\frac{1}{2}\mu L_c^2$	$\frac{3}{2}$	$\frac{1}{2}$
Case 4	1×10^6	0.3	$\frac{E}{2(1+\nu)}$	$\frac{\nu E}{(1+\nu)(1-2\nu)}$	μ	μL_c^2	μL_c^2	μL_c^2	$\frac{2}{3}$	$\frac{1}{2}$

results should be independent on the mesh density. In the current study, we held the aspect ratio as close as possible near unity and we gradually reduced the element volume. Consequently, more DOFs are expected for very fine meshes. This enables us to compare the numerical results in an identical manner under the same loading using torque-DOFs diagram. To perform this, we need to address the definition of total torque on $\partial\Omega_1$:

$$M_{\mathrm{T}} := M_{\mathrm{Tmp}}^{exact} + M_{\mathrm{Tcurv}}^{exact}, \tag{34a}$$

where

$$M_{\mathrm{Tmp}}^{exact} := \int_{\partial\Omega_1} (x_1 \bar{\sigma}_{32}^{exact} - x_2 \bar{\sigma}_{31}^{exact}) dS = \int_{\partial\Omega_1^0} (x_1 \bar{\sigma}_{32} - x_2 \bar{\sigma}_{31}) dS^0 \tag{34b}$$

and

$$M_{\mathrm{Tcurv}}^{exact} := \int_{\partial\Omega_1} m_{33}^{exact} dS = \int_{\partial\Omega_1^0} m_{33} dS^0 \tag{34c}$$

In (34b) and (34c), the superscript "0" indicates reference position. The exact stress and exact couple stress could be written as below:

$$\bar{\sigma}^{exact} = \frac{1}{det[\mathrm{F}]} S_1 \mathrm{F}^T \quad \text{and only for linear Cosserat elasticity} \quad S_1 = \bar{\sigma}, \tag{35a}$$

$$m^{exact} = \frac{1}{det[\mathrm{F}]} T_1 \mathrm{F}^T \quad \text{and only for linear Cosserat elasticity} \quad T_1 = m. \tag{35b}$$

In Fig. 6, the integrated torque on the top of Cosserat circular bar versus DOFs is displayed for case 4 including $\mu_c = \mu$ and $L_c = 1 \times 10^7$ mm. Hence, besides of the convergence issue for each computation, we observe also the mesh-independency feature, which is extremely important for the size effect-based models, notably Cosserat models. As shown in Fig. 6, M_{Tmp} and M_{Tcurv} approach to their asymptotes but the curvature stiffness-based torque is approaching to its asymptote slower than stiffness torque. This is an unwilling consequence of the application of linear shape functions for the micro-rotations as explained earlier in the paper.

By using the results obtained in Fig. 6, we have chosen one suitable and rather precise mesh density for the followed calculations, which are provided in this work. The mesh statistics and some convergence criteria have been made for the torsion test in Table 2.

In next sub-section, the boundedness properties of the aforementioned cases (case 1–4) altogether regarding the grid frameworks model assumption for the micro-rotation boundary conditions will be considered. As exhibited in Fig. 2, we fixed all micro-rotations on the bottom of the circular bar and we released only ϕ_3 on the top. The comparison among these cases in a semi-logarithmic diagram (*Torque*-Log (L_c)) will be equally treated in next sub-section.

3.2.2. Torsion test numerical experiments: boundedness and size effects comparison among all available cases

In this sub-section, we will present that the proposed micro-rotation boundary conditions or so-called artificial boundary conditions, yield the boundedness properties for all discussed cases. To achieve this, we used a fairly precise model (Table 2). We also show the outcomes in *Torque*-Log (L_c) diagram. In Fig. 7(a)–(c), stiffness-based torque M_{Tmp} and curvature stiffness-based torque M_{Tcurv} are plotted versus ϑ as a computation history diagram. Indeed, each peak deals with one torsion test (ϑ between 0 and 13 degree) corresponding to a L_c value. The L_c values get started with zero and they attain 1×10^7 mm at the end of computation (0 mm, 0.001 mm, 0.01 mm, 0.1 mm, 0.2 mm, 0.3 mm, 0.4 mm, 0.5 mm, 1 mm, 5 mm, 10 mm, 100 mm, 1000 mm, 1×10^4 mm, 1×10^5 mm,1×10^6 mm,1×10^7 mm). Therefore, the first peak handles ϑ between 0 and 13 degree and $L_c = 0$ mm and second peak for $L_c = 0.001$ mm and so on. According to Fig. 7(a)–(c), we always find out the boundedness for very large L_c values. It means that the smaller specimens (large L_c values) are stiffer than bigger specimens (small L_c values). It is of importance to note that the total torque ($M_{\mathrm{T}} = M_{\mathrm{Tmp}} + M_{\mathrm{Tcurv}}$) would be also computed but it is trivial that it is bounded as like as M_{Tmp} and M_{Tcurv}. The outcomes of case 1 have not brought in this paper due to two facts, first, cases 1 and

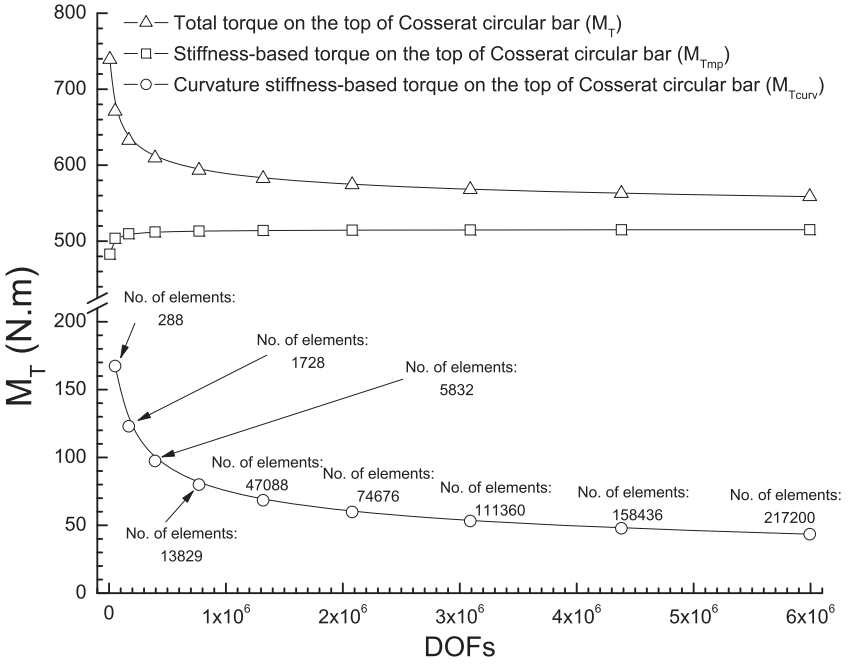

Fig. 6. Mesh-independency issue for linear Cosserat elasticity involving unit mesh aspect ratio assumption for case 4 $\left(L_c = 1 \times 10^7 \text{ mm},\ \mu_c = \mu \text{ and } \vartheta = \frac{13\pi}{180}\right)$.

Table 2
Mesh statistics and relative error for the 3D-FEM analysis of torsion test.

Element type	No. of nodes	No. of elements	DOFs	Elements aspect ratio	Relative error
28-node brick	6655	5832	169,404	1	1×10^{-6}

2 are identical, second, case 1 suffers from some numerical convergences (it is necessary to switch to a direct solver rather than an iterative solver (consequently, it drastically increases runtime)) and μ_c and L_c dependency problem. Furthermore, case 1 coincides with the 2D Cosserat models whose considerations are less valuable due to the fact that we solely use gradient of micro-rotation ($\nabla\phi$) in the second constitutive law.

We readily distinguish the boundedness property for all cases involving grid framework assumption for micro-rotations. The comparison among all cases nearly represents the same global behavior for cases 1, 2 and 4 but conformal case 3 is quite different. The major difference arises from the fact that it can bear more curvature torque for the same L_c values comparing to the others.

In Fig. 8(a)–(c), all cases are equally compared in a semi-logarithmic diagram or so-called *Torque*-Log (L_c) diagram. The global behavior of cases 2 and 4 are approximately identical and conformal case 3 behaves differently.[13]

We can distinct three zones in *Torque*-Log (L_c) diagram:

- Zone I: Model behaves as like as classical Cauchy-Boltzmann's media, i.e. no size effects,
- Zone II: Model is completely size dependent,
- Zone III: Lack of size effects for very large L_c values was observed.

As illustrated in Fig. 8a(a)–(c), three zones appear in the semi-logarithmic diagram. The first and last zones are non-size effect affected zones, whereas, zone II is entirely a size effect affected zone. Cases 2 and 4 as well as case 1 display identical L_c values for the start point (L_c = 0.1 mm) and end point of zone II (L_c = 100 mm). Alternatively, conformal case 3 enlarges the size effect affected zone. Accordingly, more size effects must be expected for this case. It is well worth serious consideration and is named *Conformal case* in which we can expect the *heterogeneous deformations* [4]. Surprisingly, M_{Tcurv} attains the values greater than those found for stiffness torque M_{Tmp} in case 2, case 4 and conformal case 3 by itself! Indeed, it takes place due to the intrinsic feature of conformality and heterogeneous deformation concept whose utilization for the heterogeneous media looks like very interesting and it should be followed by a comprehensive study.

[13] It is straightforward to emphasize that case 1 makes some numerical problems using iterative solver, especially for the values less than 0.5 mm. To overcome this disadvantage, we used a direct solver. The same phenomenon was found out by an independent user-written FEM code either [62].

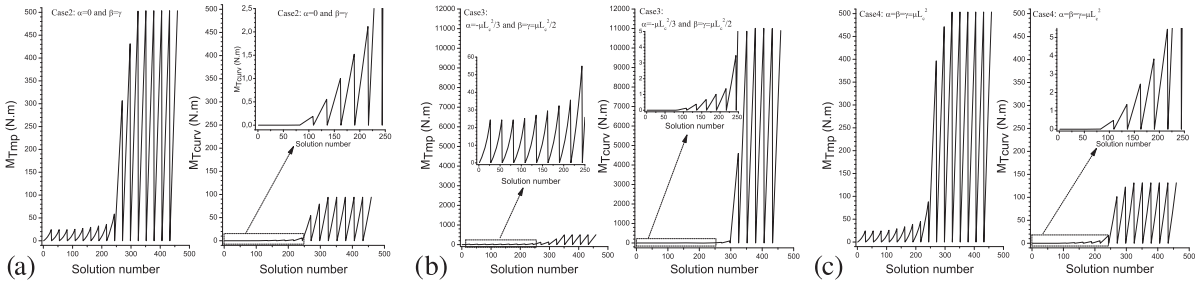

Fig. 7. (a) Computation history results for case 2 $\left(\alpha = 0 \text{ and } \beta = \gamma = \frac{\mu L_c^2}{2}\right)$: M_{Tmp} and M_{Tcurv} versus solution number. Every peak represents the angle of torsion between 0 and 13 degree, i.e. $0 \leqslant \vartheta \leqslant \frac{13\pi}{180}$ for a specific L_c value (0 mm, 0.001 mm, 0.01 mm, 0.1 mm, 0.2 mm, 0.3 mm, 0.4 mm, 0.5 mm, 1 mm, 5 mm, 10 mm, 100 mm, 1000 mm, 1×10^4 mm, 1×10^5 mm, 1×10^6 mm, 1×10^7 mm), (b) Computation history results for conformal case 3 $\left(\alpha = -\frac{\mu L_c^2}{3} \text{ and } \beta = \gamma = \frac{\mu L_c^2}{2}\right)$: M_{Tmp} and M_{Tcurv} versus solution number. Every peak represents the angle of torsion between 0 and 13 degree, i.e. $0 \leqslant \vartheta \leqslant \frac{13\pi}{180}$ for a specific L_c value (0 mm, 0.001 mm, 0.01 mm, 0.1 mm, 0.2 mm, 0.3 mm, 0.4 mm, 0.5 mm, 1 mm, 5 mm, 10 mm, 100 mm, 1000 mm, 1×10^4 mm, 1×10^5 mm, 1×10^6 mm, 1×10^7 mm), (c) Computation history results for case 4 $\left(\alpha = \beta = \gamma = \mu L_c^2\right)$: M_{Tmp} and M_{Tcurv} versus solution number. Every peak represents the angle of torsion between 0 and 13 degree, i.e. $0 \leqslant \vartheta \leqslant \frac{13\pi}{180}$ for a specific L_c value (0 mm, 0.001 mm, 0.01 mm, 0.1 mm, 0.2 mm, 0.3 mm, 0.4 mm, 0.5 mm, 1 mm, 5 mm, 10 mm, 100 mm, 1000 mm, 1×10^4 mm, 1×10^5 mm, 1×10^6 mm, 1×10^7 mm).

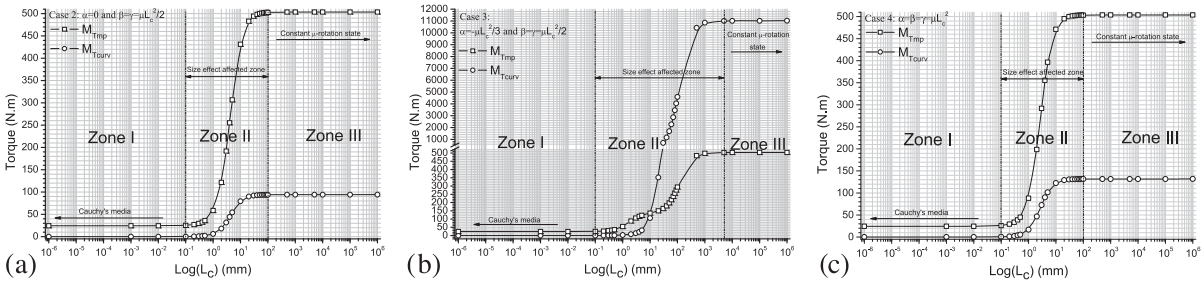

Fig. 8. (a) Semi-logarithmic diagram of Torque versus Log (L_c) including stiffness torque (M_{Tmp}) and curvature stiffness torque (M_{Tcurv}) for case 2 $\left(\alpha = 0 \text{ and } \beta = \gamma = \frac{\mu L_c^2}{2}\right)$ and $\vartheta = \frac{13\pi}{180}$, (b) Semi-logarithmic diagram of Torque versus Log (L_c) including stiffness torque (M_{Tmp}) and curvature stiffness torque (M_{Tcurv}) for conformal case 3 $\left(\alpha = -\frac{\mu L_c^2}{3} \text{ and } \beta = \gamma = \frac{\mu L_c^2}{2}\right)$ and $\vartheta = \frac{13\pi}{180}$, (c) Semi-logarithmic diagram of Torque versus Log (L_c) including stiffness torque (M_{Tmp}) and curvature stiffness torque (M_{Tcurv}) for case 4 $\left(\alpha = \beta = \gamma = \mu L_c^2\right)$ and $\vartheta = \frac{13\pi}{180}$.

Comparison among Fig. 8a, b and c, reveals that only the end point of zone II has been shifted toward higher L_c values and the start point of zone II is untouched.

The global behavior of the above-mentioned semi-logarithmic diagrams could be interpreted by the combination of matrix and grid framework assumptions. While we take into account a very large specimen, the grid frameworks cannot manipulate the global mechanical behavior (zone I), whereas the size effect can be seen when the specimen is getting smaller and smaller (zone II). When the specimen is smaller than the grid frameworks, we will miss size effects again (zone III) [5] and we obtain the constant micro-rotations. *This zone is coincided with the couple stress theory or so-called indeterminate couple stress theory. It means that the micro-rotation is no longer independent variable* [4,5].

4. Conclusions and outlooks

We can summarize some interesting conclusions and outlooks as below:

1. We can also find out the stiffness boundedness for case 4 as well as other cases (case 1, case 2, conformal case 3) involving the grid framework models assumptions for micro-rotations,
2. The boundedness property has been observed for the stiffness as well as curvature stiffness whatever case number (case 1, case 2, conformal case 3 and case 4),
3. An interesting missing part which was neglected in the Cosserat theory, has been introduced into the Cosserat theory under virtual work framework,
4. The above-mentioned term can explicitly describe the presence of m_{33} on the top of specimen, whereas we did not apply any surface couple ($Q^{(n)}$),

5. The *physical interpretation* of couple stress or so called stress moment $(m = m_{ij}\hat{e}_i \otimes \hat{e}_j)$ *must be revised* due to the fact that it contains not only the surface couple $(Q^{(n)})$ but also $r \times t^{(n)}$. Hence, stress moment second-rank tensor is affected by anti-symmetrical counterpart of stress tensor $(e : \bar{\sigma})$ as well as the impact of applied forces on the moments on the boundaries, e.g. $r \times t^{(n)}$ on Ω_t in our case (Fig. 1),
6. The semi-logarithmic diagram has been used and three specific zones based on the L_c values have been found out. This diagram makes it possible to use Cosserat theory as a multi-scale tool due to the presence of three zones including different L_c values by considering the Representative Elementary Volume (REV) concept like those done earlier in [74] via hygro-Cosserat theory using Duhamel–Neumann deformation decomposition for multi-disciplinary studies [101],
7. We can equally find out the three specific zones for stiffness torque M_{Tmp} and curvature torque M_{Tcurv} as well,
8. Conformal case 3 which was originally proposed by Neff–Jeong [4] is still very interesting so far. It is because of the fact that the curvature stiffness is several times greater than stiffness and it is substantiated that we attain the heterogeneous deformations using a continuum model [4,86,102,85],
9. By assuming the Cosserat theory as an explicit multi-scale approach (We can assume that stress tensor handles the *macro-deformations* and couple stress or stress moment deals with the *micro-deformations* under *a simplified form*, i.e. *micro-rotation*), we distinguish that it is necessary to achieve material characterization in macro-scale and micro-scale as well. Hence, the major attempts should be focused on the micro-structural material characterization by means of the rather modern tools, e.g. nano-indentation and Electron BackScattered Diffraction (EBSD) or BackScattered Kikuchi Diffraction (BKD).

Appendix A. Virtual work for Cauchy–Boltzmann's or so-called classical media

Let's take the virtual work for Cauchy–Boltzmann's media, the integration over $\partial\Omega_t$ can be replaced by $\partial\,\Omega$ due to the fact that $\delta u_i = 0$ on $\partial\Omega_u$ and $t_{ij}^{(n)} = 0$ on $\partial\Omega_0 \cup \partial\Omega_c$:

$$\int_{\Omega} \sigma^T : \delta\varepsilon\, dV = \int_{\partial\Omega} t^{(n)} \cdot \delta u\, dS + \int_{\Omega} \rho b \cdot \delta u\, dV, \tag{A.1a}$$

where

$$\int_{\partial\Omega} t^{(n)} \cdot \delta u\, dS = \int_{\partial\Omega} (\sigma^T \cdot n) \cdot \delta u\, dS = \int_{\partial\Omega} (\sigma \cdot \delta u) \cdot n\, dS = \int_{\Omega} \mathrm{Div}\,(\sigma \cdot \delta u) dV = \int_{\Omega} (\mathrm{Div}\,\sigma \cdot \delta u + \sigma : \delta(\nabla u)^T)\, dV. \tag{A.1b}$$

We know that $X^T : Y = X : Y^T$ for $\forall X, Y \in \mathbb{R}^3 \times \mathbb{R}^3$, then:

$$\int_{\partial\Omega} t^{(n)} \cdot \delta u dS = \int_{\Omega} (\mathrm{Div}\,\sigma \cdot \delta u + \sigma^T : \delta\nabla u)\, dV = \int_{\Omega} (\mathrm{Div}\,\sigma \cdot \delta u + \sigma^T : \nabla\delta u)\, dV. \tag{A.2}$$

The term $\int_{\Omega} \sigma^T : \delta\varepsilon\, dV$ can be rewritten in function of ∇u as:

$$\int_{\Omega} \sigma^T : \delta\varepsilon\, dV = \frac{1}{2}\int_{\Omega} \sigma^T : \delta(\nabla u + \nabla u^T) dV = \frac{1}{2}\int_{\Omega} \sigma^T : (\delta\nabla u + \delta(\nabla u)^T) dV = \frac{1}{2}\int_{\Omega} (\sigma^T : \delta\nabla u + \sigma^T : \delta(\nabla u)^T)\, dV. \tag{A.3}$$

We know that $X^T : Y^T = X : Y$ for $\forall X, Y \in \mathbb{R}^3 \times \mathbb{R}^3$ and by using the symmetry property for stress tensor, i.e. $\sigma^T = \sigma$ then:

$$\int_{\Omega} \sigma^T : \delta\varepsilon\, dV = \frac{1}{2}\int_{\Omega} (\sigma^T : \delta\nabla u + \sigma : \delta(\nabla u)^T)\, dV = \frac{1}{2}\int_{\Omega} (\sigma^T : \delta\nabla u + \sigma^T : \delta\nabla u)\, dV = \int_{\Omega} \sigma^T : \nabla\delta u\, dV. \tag{A.4}$$

By substituting (A.2) and (A.4) into (A.1a), we obtain the following equation:

$$\int_{\Omega} \sigma^T : \delta\varepsilon\, dV = \int_{\partial\Omega} t^{(n)} \cdot \delta u dS + \int_{\Omega} \rho b \cdot \delta u\, dV \Rightarrow \int_{\Omega} \sigma^T : \nabla\delta u\, dV = \int_{\Omega} (\mathrm{Div}\,\sigma \cdot \delta u + \sigma^T : \nabla\delta u)\, dV + \int_{\Omega} \rho b \cdot \delta u\, dV, \tag{A.5}$$

then

$$\int_{\Omega} (\mathrm{Div}\,\sigma + \rho b) \cdot \delta u\, dV = 0 \Rightarrow \mathrm{Div}\,\sigma + \rho b = 0 \quad \text{in} \quad \Omega. \tag{A.6}$$

Accordingly, we can describe the governing equations for the Cauchy-Boltzmann's media as following:

$$\mathrm{Div}\,\sigma + \rho b = 0 \quad \text{in} \quad \Omega, \tag{A.7a}$$

$$\sigma^T \cdot n = t^{(n)} \quad \text{on} \quad \partial\Omega_t \quad \text{and} \quad \sigma^T \cdot n = 0 \quad \text{on} \quad \partial\Omega_0 \cup \Omega_c. \tag{A.7b}$$

It is of importance to remind that in this case, there is no surface couple $\left(Q_{ij}^{(n)} = 0\right)$.

Appendix B. Non-negativity of the Cosserat energy density

The positive definiteness property of isotropic Cosserat elasticity can be handled for the fourth-rank stiffness tensor (D_{ijkl}) leading to the following mathematical expressions:

$$\bar{\sigma}_{ij} = (\mu + \mu_c)\bar{\varepsilon}_{ij} + (\mu - \mu_c)\bar{\varepsilon}_{ji} + \lambda\bar{\varepsilon}_{kk}\delta_{ij}, \tag{B.1a}$$

or

$$\mathbf{D} = \begin{pmatrix} \lambda+2\mu & \lambda & \lambda & 0 & 0 & 0 & 0 & 0 & 0 \\ \lambda & \lambda+2\mu & \lambda & 0 & 0 & 0 & 0 & 0 & 0 \\ \lambda & \lambda & \lambda+2\mu & 0 & 0 & 0 & 0 & 0 & 0 \\ 0 & 0 & 0 & \mu+\mu_c & \mu-\mu_c & 0 & 0 & 0 & 0 \\ 0 & 0 & 0 & \mu-\mu_c & \mu+\mu_c & 0 & 0 & 0 & 0 \\ 0 & 0 & 0 & 0 & 0 & \mu+\mu_c & \mu-\mu_c & 0 & 0 \\ 0 & 0 & 0 & 0 & 0 & \mu-\mu_c & \mu-\mu_c & 0 & 0 \\ 0 & 0 & 0 & 0 & 0 & 0 & 0 & \mu+\mu_c & \mu-\mu_c \\ 0 & 0 & 0 & 0 & 0 & 0 & 0 & \mu-\mu_c & \mu+\mu_c \end{pmatrix}. \tag{B.1b}$$

To obtain the bounds of the material constants, we should verify the determinant of diagonal matrices as:

$$\det(D)_{1\times1} > 0 \Rightarrow \lambda + 2\mu > 0, \tag{B.2a}$$

$$\det(D)_{2\times2} > 0 \Rightarrow 4\mu(\mu + \lambda) > 0, \tag{B.2b}$$

$$\det(D)_{3\times3} > 0 \Rightarrow 4\mu^2(3\lambda + 2\mu) > 0, \tag{B.2c}$$

$$\det(D)_{4\times4} > 0 \Rightarrow 4\mu^2[\mu(3\lambda + 2\mu) + \mu_c(\lambda + 2\mu)] > 0, \tag{B.2d}$$

$$\det(D)_{5\times5} > 0 \Rightarrow 16\mu^3\mu_c(3\lambda + 2\mu) > 0, \tag{B.2e}$$

$$\det(D)_{6\times6} > 0 \Rightarrow 16\mu^3\mu_c(3\lambda + 2\mu)(\mu + \mu_c) > 0, \tag{B.2f}$$

$$\det(D)_{7\times7} > 0 \Rightarrow 64\mu^4\mu_c^2(3\lambda + 2\mu) > 0, \tag{B.2g}$$

$$\det(D)_{8\times8} > 0 \Rightarrow 64\mu^4\mu_c^2(3\lambda + 2\mu)(\mu + \mu_c) > 0, \tag{B.2h}$$

$$\det(D)_{9\times9} > 0 \Rightarrow 128\mu^4\mu_c^3(3\lambda + 2\mu)(\mu + \mu_c) > 0. \tag{B.2i}$$

Therefore, the following restrictions could be concluded:

$$3\lambda + 2\mu > 0, \quad \mu + \mu_c > 0, \quad \mu_c > 0, \quad \mu > 0, \quad \lambda + \mu > 0, \quad \lambda + 2\mu > 0. \tag{B.3}$$

We can simplify further as:

$$3\lambda + 2\mu > 0, \quad \mu > 0, \quad \mu_c > 0. \tag{B.4}$$

The positive definiteness property of isotropic Cosserat elasticity can be handled for the fourth-rank curvature stiffness tensor (E_{ijkl}) leading to the following mathematical expressions:

$$m_{ij} = \beta\bar{k}_{ij} + \gamma\bar{k}_{ji} + \alpha\bar{k}_{kk}\delta_{ij} \tag{B.5}$$

and

$$\mathbf{E} := \begin{pmatrix} \alpha+\beta+\gamma & \alpha & \alpha & 0 & 0 & 0 & 0 & 0 & 0 \\ \alpha & \alpha+\beta+\gamma & \alpha & 0 & 0 & 0 & 0 & 0 & 0 \\ \alpha & \alpha & \alpha+\beta+\gamma & 0 & 0 & 0 & 0 & 0 & 0 \\ 0 & 0 & 0 & \gamma & \beta & 0 & 0 & 0 & 0 \\ 0 & 0 & 0 & \beta & \gamma & 0 & 0 & 0 & 0 \\ 0 & 0 & 0 & 0 & 0 & \gamma & \beta & 0 & 0 \\ 0 & 0 & 0 & 0 & 0 & \beta & \gamma & 0 & 0 \\ 0 & 0 & 0 & 0 & 0 & 0 & 0 & \gamma & \beta \\ 0 & 0 & 0 & 0 & 0 & 0 & 0 & \beta & \gamma \end{pmatrix}. \tag{B.6}$$

We should equally verify the determinant of diagonal matrices as below:

$$\det(E)_{1\times1} > 0 \Rightarrow \alpha+\beta+\gamma > 0, \tag{B.7a}$$

$$\det(E)_{2\times2} > 0 \Rightarrow (\beta+\gamma)(2\alpha+\beta+\gamma) > 0, \tag{B.7b}$$

$$\det(E)_{3\times3} > 0 \Rightarrow (3\alpha+\beta+\gamma)(\beta+\gamma)^2 > 0, \tag{B.7c}$$

$$\det(E)_{4\times4} > 0 \Rightarrow \gamma(\beta+\gamma)^2(3\alpha+\beta+\gamma) > 0, \tag{B.7d}$$

$$\det(E)_{5\times5} > 0 \Rightarrow (\beta+\gamma)^3(3\alpha+\beta+\gamma)(\gamma-\beta) > 0, \tag{B.7e}$$

$$\det(E)_{6\times6} > 0 \Rightarrow \gamma(\beta+\gamma)^3(3\alpha+\beta+\gamma)(\gamma-\beta) > 0, \tag{B.7f}$$

$$\det(E)_{7\times7} > 0 \Rightarrow (\beta+\gamma)^4(3\alpha+\beta+\gamma)(\gamma-\beta)^2 > 0, \tag{B.7g}$$

$$\det(E)_{8\times8} > 0 \Rightarrow \gamma(\beta+\gamma)^4(3\alpha+\beta+\gamma)(\gamma-\beta)^2 > 0, \tag{B.7h}$$

$$\det(E)_{9\times9} > 0 \Rightarrow (\beta+\gamma)^5(3\alpha+\beta+\gamma)(\gamma-\beta)^3 > 0. \tag{B.7i}$$

Hence, the following restrictions could be concluded for the couple stress-micropolar curvature tensor constitutive law:

$$3\alpha+\beta+\gamma > 0, \quad \alpha+\beta+\gamma > 0, \quad \gamma > 0, \quad (\gamma+\beta)^3(\gamma-\beta) > 0. \tag{B.8}$$

We can rewrite them under the simplified form:

$$3\alpha+\beta+\gamma > 0, \quad \beta+\gamma > 0, \quad \gamma-\beta > 0, \quad \gamma > 0. \tag{B.9}$$

Appendix C. Total energy density at a glance

The total energy density excluding the zero-centrosymmetrical part for elastic isotropic materials can be represented as the following forms:

$$\begin{aligned} W(\bar{\varepsilon}_{ij},\bar{k}_{ij}) &:= W_{\mathrm{mp}}(\bar{\varepsilon}_{ij},\bar{k}_{ij}) + W_{\mathrm{curv}}(\bar{\varepsilon}_{ij},\bar{k}_{ij}) = \frac{1}{2}\bar{\sigma}^T : \bar{\varepsilon} + \frac{1}{2}m^T : \bar{k} \\ &= \frac{1}{2}\left(2\mu\|\mathrm{sym}\,\bar{\varepsilon}\|^2 + 2\mu_c\|\mathrm{skew}\bar{\varepsilon}\|^2 + \lambda\mathrm{tr}[\bar{\varepsilon}]^2\right) + \frac{1}{2}\left((\beta+\gamma)\|\mathrm{sym}\,\bar{k}\|^2 + (\beta-\gamma)\|\mathrm{skew}\bar{k}\|^2 + \alpha\mathrm{tr}[\bar{k}]^2\right) \\ &= \frac{1}{2}\left(2\mu\|\mathrm{dev}\,\mathrm{sym}\,\bar{\varepsilon}\|^2 + 2\mu_c\|\mathrm{skew}\bar{\varepsilon}\|^2 + \frac{2\lambda+3\mu}{6}\mathrm{tr}[\bar{\varepsilon}]^2\right) \\ &\quad + \frac{1}{2}\left((\beta+\gamma)\|\mathrm{dev}\,\mathrm{sym}\,\bar{k}\|^2 + (\beta-\gamma)\|\mathrm{skew}\bar{k}\|^2 + \frac{3\alpha+(\beta+\gamma)}{6}\mathrm{tr}[\bar{k}]^2\right). \end{aligned} \tag{C.1}$$

It is important to note that:

$$X : X = X_{ij}X_{ij} = \|X\|^2_{\mathbb{R}^3\times\mathbb{R}^3} = \|X\|^2, \quad \forall X \in \mathbb{R}^3\times\mathbb{R}^3, \tag{C.2a}$$

$$\|\mathrm{dev}\,\mathrm{sym}X\|^2 = \|\mathrm{sym}X\|^2 - \frac{1}{3}\mathrm{tr}[\mathrm{sym}X]^2 = \|\mathrm{sym}X\|^2 - \frac{1}{3}\mathrm{tr}[X]^2, \quad \forall X \in \mathbb{R}^3\times\mathbb{R}^3. \tag{C.2b}$$

Appendix D. Notations

Let $\Omega \subset \mathbb{R}^3$ be a bounded domain with Lipschitz boundary.$\partial\Omega$ and let Γ be a smooth subset of $\partial\Omega$ with non-vanishing 2-dimensional Hausdorff measure. For $a, b \in \mathbb{R}^3$ we let $a \cdot b$ denote the scalar product on $\mathbb{R}^3$ with associated vector norm $\|a\|^2_{R^3} = a \cdot b = a_i b_i$ for $i = 1,2,3$ where $i \in \mathbb{N}$. We denote by $\mathbb{M}^{3\times3}$ or $\mathbb{R}^3 \times \mathbb{R}^3$ the set of real 3×3 s order tensors, written with capital letters and sym denotes symmetric second orders tensors. The standard Euclidean scalar product on $\mathbb{M}^{3\times3}$ is given by $\langle X, Y\rangle_{\mathbb{M}^{3\times3}} = X : Y = \mathrm{tr}XY^T = \mathrm{tr}X^TY = X_{ij}Y_{ij}$ for $i,j = 1,2,3$where $i,j \in \mathbb{N}$, and thus the Frobenius tensor norm is $\|X\|^2 = X : X = \langle X, X\rangle_{\mathbb{M}^{3\times3}}$. In the following we omit the index $\mathbb{R}^3, \mathbb{M}^{3\times3}$. The identity tensor on $\mathbb{M}^{3\times3}$ will be denoted by $\mathbb{I}$, so that $\mathrm{tr}X = \langle X, \mathbb{I}\rangle = X : \mathbb{I} = X_{ij}\delta_{ij}$ for $i,j = 1,2,3$ where $i,j \in \mathbb{N}$. We denote the scalar product of permutation tensor (third-rank tensor) e_{ijk} and a second-rank tensor X, so that $\mathbf{e} \cdot X = e_{ijk}X_{kl}\hat{e}_i \otimes \hat{e}_j \otimes \hat{e}_l$ and $\mathbf{e} : X = e_{ijk}X_{jk}\hat{e}_i$. The gradient of a vector can be denoted so that $\nabla a = a_{j,i}\hat{e}_i \otimes \hat{e}_j$ where $\nabla a \in \mathbb{M}^{3\times3}$ We set $\mathrm{sym}\,(X) = \frac{1}{2}(X^T + X)$ and $\mathrm{skew}(X) = \frac{1}{2}(X - X^T)$ such that X = sym (X) + skew (X) where $X \in \mathbb{M}^{3\times3}$. For $X \in \mathbb{M}^{3\times3}$ we set for the deviatoric part $\mathrm{dev}X = X - \frac{1}{3}\,\mathrm{tr}X\mathbb{I} \in \mathfrak{sl}(3)$ where $\mathfrak{sl}(3)$ is the Lie-algebra of traceless matrices. The set Sym (n) denotes all symmetric $n \times n$-matrices.

The Lie-algebra of SO $(3) := \{X \in \mathrm{GL}\,(3) | X^TX = \mathbb{I}, \det X = 1\}$ is given by the set $\mathfrak{so}(3) := \{X \in \mathbb{M}^{3\times3} | X^T = -X\}$ of all skew symmetric tensors. The canonical identification of $\mathfrak{so}(3)$ and $\mathbb{R}^3$ is denoted by $\mathrm{ax}\overline{A} \in \mathbb{R}^3$ for $\overline{A} \in \mathfrak{so}(3)$. Note that $(\mathrm{ax}\overline{A}) \times \xi = \overline{A} \cdot \xi$ for all $\xi \in \mathbb{R}^3$, such that

$$\mathrm{axl}\begin{pmatrix} 0 & \alpha & \beta \\ -\alpha & 0 & \gamma \\ -\beta & -\gamma & 0 \end{pmatrix} := \begin{pmatrix} -\gamma \\ \beta \\ -\alpha \end{pmatrix}, \tag{D.1}$$

$$\overline{A}_{ij} = \sum_{k=1}^{3} -\varepsilon_{ijk} \cdot \mathrm{axl}\overline{A}_k,$$
$$\|\overline{A}\|^2_{\mathbb{M}^{3\times3}} = 2\|\mathrm{axl}\overline{A}\|^2_{\mathbb{R}^3},$$
$$\langle \overline{A}, \overline{B}\rangle_{\mathbb{M}^{3\times3}} = 2\langle \mathrm{axl}\overline{A},\ \mathrm{axl}\overline{B}\rangle_{\mathbb{R}^3}.$$

Under the Einstein's summation convention, the dual vector (axl) and dual tensor (anti) could be shown as below:

$$X := \mathrm{anti}x = -x_i e_{ijk}\hat{e}_j \otimes \hat{e}_k = -x \cdot \mathbf{e} \text{ where } x \in \mathbb{R}^3 \text{ and } X \in \mathbb{M}^{3\times3}, \tag{D.3a}$$

$$x := \mathrm{axl}X = -\frac{1}{2} e_{ijk} X_{jk} \hat{e}_i = -\frac{1}{2}\mathbf{e} : X \text{ where } x \in \mathbb{R}^3 \text{ and } X \in \mathbb{M}^{3\times3}. \tag{D.3b}$$

References

[1] Z.P. Bazant, Micropolar medium as a model for buckling of grid frameworks, in: Proceedings of 12th Midwestern Mechanics Conference on Developments in Mechanics, vol. 6, 1971, pp. 587–593.
[2] Z.P. Bazant, M. Christensen, Analogy between micropolar continuum and grid frameworks under initial stress, Int. J. Solids Struct. 8 (3) (1972) 327–346.
[3] Jena Jeong, Patrizio Neff, Existence, uniqueness and stability in linear Cosserat elasticity for weakest curvature conditions, Math. Mech. Solids 15 (1) (2010) 78–95, doi:10.1177/1081286508093581. First published on September 17, 2008.
[4] P. Neff, J. Jeong, A new paradigm: the linear isotropic Cosserat model with conformally invariant curvature energy, Z. Angew. Math. Mech. 89 (2) (2009) 107–122.
[5] J. Jeong, H. Ramézani, I. Münch, P. Neff, Simulation of linear isotropic Cosserat elasticity with conformally invariant curvature, Z. Angew. Math. Mech. 89 (7) (2009) 552–569.
[6] Z.P. Bazant, G. Pijaudier-Cabot, Measurement of characteristic length of non-local continuum, J. Eng. Mech., ASCE 115 (4) (1989) 755–767.
[7] G. Pijaudier-Cabot, Z.P. Bazant, Non-local damage theory, J. Eng. Mech., ASCE 113 (10) (1987) 1512–1533.
[8] E. Papamichos, I. Vardoulakis, H.-B. Mühlhaus, Buckling of layered elastic media: a cosserat-continuum approach and its validation, Int. J. Numer. Anal. Methods Geomech. 14 (7) (1990) 473–498.
[9] R. de Borst, L.J. Sluys, Localisation in a Cosserat continuum under static and dynamic loading conditions, Comput. Methods Appl. Mech. Eng. 90 (1–3) (1991) 805–827.
[10] R.H.J. Peerlings, R. de Borst, W.A.M. Brekelmans, M.G.D. Geers, Localization issues in local and nonlocal continuum approaches to fracture, Eur. J. Mech., A/Solids 21 (2) (2002) 75–189.
[11] J.P. Bardet, J. Proubet, A numerical investigation of the structure of persistent shear band in granular media, Géotechnique 41 (4) (1992) 599–613.
[12] Maria-Magdalena Iordache, Kaspar Willam, Localized failure analysis in elastoplastic Cosserat continua, Comput. Methods Appl. Mech. Eng. 151 (3–4) (1998) 559–586.
[13] E. Bauer, Analysis of shear band bifurcation with a hypoelastic model for a pressure and density sensitive granular material, Mech. Mater. 31 (9) (1999) 597–609.
[14] J. Tejchman, G. Gudehus, Shearing of a narrow granular layer with polar quantities, Int. J. Numer. Anal. Methods Geomech. 25 (1) (2001) 1–28.
[15] Majid T. Manzari, Application of micropolar plasticity to post failure analysis in geomechanics, Int. J. Numer. Anal. Methods Geomech. 28 (10) (2004) 1011–1032.
[16] Th. Maier, Comparison of non-local and polar modelling of softening in hypoplasticity, Int. J. Numer. Anal. Methods Geomech. 28 (3) (2004) 2004.
[17] Khalid A. Alshibli, Mustafa I. Alsaleh, George Z. Voyiadjis, Modelling strain localization in granular materials using micropolar theory: mathematical formulations, Int. J. Numer. Anal. Methods Geomech. 30 (15) (2006) 1501–1524.
[18] Azadeh Riahi, John H. Curran, Full 3d finite element Cosserat formulation with application in layered structures, Appl. Math. Model. 33 (8) (2009) 3450–3464.
[19] A. Riahi, J.H. Curran, H. Bidhendi, Buckling analysis of 3d layered structures using a Cosserat continuum approach, Comput. Geotech. 36 (7) (2009) 1101–1112.
[20] Jena Jeong, Hamidréza Ramézani, Enhanced numerical study of infinitesimal non-linear Cosserat theory based on the grain size length scale assumption, Comput. Methods Appl. Mech. Eng. 199 (45–48) (2010) 2892–2902.
[21] K. Karimi, A.R. Khoei, On the analysis of simple shear problem using the micro-polar hypoelasticity Cosserat theory, Eur. J. Mech. – A/Solids 29 (4) (2010) 664–674.
[22] A.R. Khoei, S. Yadegari, S.O.R. Biabanaki, 3d finite element modeling of shear band localization via the micro-polar Cosserat continuum theory, Comput. Mater. Sci. 49 (4) (2010) 720–733.
[23] A.R. Khoei, K. Karimi, An enriched-fem model for simulation of localization phenomenon in Cosserat continuum theory, Comput. Mater. Sci. 44 (2) (2008) 733–749.
[24] Franck J. Vernerey, Wing Kam Liu, Brian Moran, Gregory Olson, A micromorphic model for the multiple scale failure of heterogeneous materials, J. Mech. Phys. Solids 56 (4) (2008) 1320–1347.
[25] Su Hao, Wing Kam Liu, Brian Moran, Franck Vernerey, Gregory B. Olson, Multi-scale constitutive model and computational framework for the design of ultra-high strength, high toughness steels, Comput. Methods Appl. Mech. Eng. 193 (17–20) (2004) 1865–1908. Multiple Scale Methods for Nanoscale Mechanics and Materials.
[26] Franck Vernerey, Wing Kam Liu, Brian Moran, Gregory Olson, Multi-length scale micromorphic process zone model, Comput. Mech. 44 (2009) 433–445, doi:10.1007/s00466-009-0382-7.
[27] E. Cosserat, F. Cosserat, Théorie des corps déformables, Librairie Scientifique A, Hermann et Fils (English translation by D. Delphenich 2007), Paris, 1909.
[28] W. Günther, Zur statik und kinematik des cosseratschen kontinuums, Abh. Braunschweig Wiss. Ges. 10 (1958) 195–213 (in German).
[29] R.D. Mindlin, H.F. Tiersten, Effects of couple stresses in linear elasticity, Arch. Rat. Mech. Anal. 11 (1962) 415–447.
[30] R.D. Mindlin, Second gradient of strain and surface tension in linear elasticity, Int. J. Solids Struct. 1 (1965) 417–438.
[31] A.C. Eringen, E.S. Suhubi, Nonlinear theory of simple micro-elastic solids, Int. J. Eng. Sci. 2 (1964) 189–203.
[32] A.C. Eringen, Theory of micropolar fluids, J. Math. Mech. 16 (1966) 1–18.

[33] A.C. Eringen, Theory of micropolar plates, Z. Angew. Math. Phys. 18 (1967) 12–30.
[34] A.C. Eringen, Theory of micropolar elasticity, in: H. Liebowitz (Ed.), Fracture An Advanced Treatise, vol. II, Academic Press, New York, 1968, pp. 621–729.
[35] S. Cowin, An incorrect inequality in micropolar elasticity theory, Z. Angew. Math. Phys. 21 (1970) 494–497.
[36] A.C. Eringen, C.B. Kafadar, Polar field theories, in: A.C. Eringen (Ed.), Continuum Physics, Polar and Nonlocal Field Theories, vol. IV, Academic Press, New York, 1976, pp. 1–73.
[37] A.C. Eringen, Microcontinuum Field Theories, Springer, Heidelberg, 1999.
[38] Amin Moosaie, Gholamali Atefi, Cosserat modeling of turbulent plane-couette and pressure-driven channel flows, J. Fluids Eng., ASME 129 (2007) 806–810.
[39] R.A. Toupin, Elastic materials with couple stresses, Arch. Rat. Mech. Anal. 11 (1962) 385–413.
[40] R.A. Toupin, Theory of elasticity with couple stresses, Arch. Rat. Mech. Anal. 17 (1964) 85–112.
[41] R.S. Lakes, Cosserat micromechanics of human bone: strain redistribution by a hydration-sensitive constituent, J. Biomech. 19 (5) (1986) 385–397.
[42] R.S. Lakes, S. Nakamura, J.C. Behiri, W. Bonfield, Fracture mechanics of bone with short cracks, J. Biomech. 23 (10) (1990) 967–975.
[43] R.S. Lakes, A pathological example in micropolar elasticity, ASME J. Appl. Mech. 52 (1985) 234–235.
[44] H.C. Park, R.S. Lakes, Torsion of a micropolar elastic prism of square cross section, Int. J. Solids Struct. 23 (1987) 485–503.
[45] W.B. Anderson, R.S. Lakes, Size effects due to Cosserat elasticity and surface damage in closed-cell polymethacrylimide foam, J. Mater. Sci. 29 (1994) 6413–6419.
[46] Cihan Tekoglu, Patrick R. Onck, Size effects in two-dimensional Voronoi foams: a comparison between generalized continua and discrete models, J. Mech. Phys. Solids 56 (12) (2008) 3541–3564.
[47] Gengkai Hu, Xiaoning Liu, Tian Jian Lu, A variational method for non-linear micropolar composites, Mech. Mater. (4) (2005) 407–425.
[48] H.W. Zhang, H. Wang, J.B. Wang, Parametric variational principle based elastic-plastic analysis of materials with polygonal and Voronoi cell finite element methods, Finite Elem. Anal. Design 43 (3) (2007) 206–217.
[49] H.W. Zhang, H. Wang, B.S. Chen, Z.Q. Xie, Analysis of Cosserat materials with Voronoi cell finite element method and parametric variational principle, Comput. Methods Appl. Mech. Eng. 197 (6–8) (2008) 741–755.
[50] H.W. Zhang, H. Wang, P. Wriggers, B.A. Schrefler, A finite element method for contact analysis of multiple Cosserat bodies, Comput. Mech. 36 (6) (2005) 444–458.
[51] E. Providas, M.A. Kattis, Finite element method in plane Cosserat elasticity, Comput. Struct. 80 (2002) 2059–2069.
[52] S. Forest, G. Cailletaud, R. Sievert, A Cosserat theory for elastoviscoplastic single crystals at finite deformation, Arch. Mech. 49 (4) (1997) 705–736.
[53] R. Dendievel, S. Forest, G. Canova, An estimation of overall properties of heterogeneous Cosserat materials, in: A. Bertram, F. Sidoroff (Eds.), Mechanics of Materials with Intrinsic Length Scale: Physics, Experiments, Modelling and Applications, Journal Physique IV France, vol. 8, EDP Sciences, France, 1998, pp. 111–118.
[54] S. Forest, R. Sievert, Nonlinear microstrain theories, Int. J. Solids Struct. 43 (2006) 7224–7245.
[55] M. Ristinmaa, M. Vecchi, Use of couple-stress theory in elasto-plasticity, Comput. Methods Appl. Mech. Eng. 136 (1996) 205–224.
[56] P. Neff, I. Münch, Simple shear in nonlinear Cosserat elasticity: bifurcation and induced microstructure, Continuum Mech. Thermodyn. 21 (3) (2009) 195–221.
[57] W. Pietraszkiewicz, V.A. Eremeyev, On natural strain measures of the non-linear micropolar continuum, Int. J. Solids Struct. 46 (3–4) (2009) 774–787.
[58] W. Pietraszkiewicz, V.A. Eremeyev, On vectorially parameterized natural strain measures of the non-linear Cosserat continuum, Int. J. Solids Struct. 46 (11–12) (2009) 2477–2480.
[59] S.L. Altman, Rotations, Quaternions, and Double Groups, Clarendon Press Oxford, 1986.
[60] S.N. Atluri, A. Cazzani, Rotations in computational solid mechanics, Arch. Comput. Mech. Eng. 2 (1) (1995) 49138.
[61] I. Münch, W. Wagner, P. Neff, Constitutive modeling and FEM for a nonlinear Cosserat continuum, PAMM 6 (1) (2006) 499–500.
[62] Ingo Münch, Ein geometrisch und materiell nichtlineares Cosserat–Modell–Theorie, Numerik und Anwendungsmöglichkeiten, Ph.D. Thesis, University of Karlsruhe (TH), October 2007. (in German).
[63] C. Sansour, S. Skatulla, A non-linear Cosserat continuum-based formulation and moving least square approximations in computations of size-scale effects in elasticity, Comput. Mater. Sci. 41 (4) (2008) 589–601.
[64] S. Bauer, M. Schäfer, P. Grammenoudis, Ch. Tsakmakis, Three-dimensional finite elements for large deformation micropolar elasticity, Comput. Methods Appl. Mech. Eng. 199 (41–44) (2010) 2643–2654.
[65] P. Neff, A finite-strain elastic-plastic Cosserat theory for polycrystals with grain rotations, Int. J. Eng. Sci. 44 (2006) 574–594, doi:10.1016/j.ijengsci.2006.04.002.
[66] P. Neff, S. Forest, A geometrically exact micromorphic model for elastic metallic foams accounting for affine microstructure. Modelling, existence of minimizers, identification of moduli and computational results, J. Elast. 87 (2007) 239–276.
[67] J.P. Bardet, J. Proubet, A shear band analysis in idealized granular materials, J. Eng. Mech., ASCE 118 (2) (1992) 397–415.
[68] J. Desrues, Localisation de la déformation plastique dans les matériaux granulaires, Ph.D. Thesis, University of Grenoble, 1984. (in French).
[69] R.S. Lakes, Experimental micro mechanics methods for conventional and negative poisson's ratio cellular solids as Cosserat continua, J. Mech. Design 113 (1) (1991) 148–155.
[70] R.S. Lakes, Experimental microelasticity of two porous solids, Int. J. Solids Struct. 22 (1) (1986) 55–63.
[71] D. Iesan, Torsion of micropolar elastic beams, Int. J. Eng. Sci. 9 (1971) 1047–1060.
[72] R.D. Gauthier, W.E. Jahsman, A quest for micropolar constants, ASME J. Appl. Mech. 42 (1975) 369–374.
[73] R.D. Gauthier, Experimental investigations on micropolar media, in: O. Brulin, R.K.T. Hsieh (Eds.), Mechanics of Micropolar Media, World Scientific, Singapore, 1982, pp. 395–463. CISM Lectures.
[74] Jena Jeong, Pierre Mounanga, Hamidréza Ramézani, Marwen Bouasker, A new multi-scale modeling approach based on hygro-cosserat theory for self-induced stress in hydrating cementitious mortars, Comput. Mater. Sci. 50 (7) (2011) 2063–2074.
[75] J.H. Heinbockel, Introduction to Tensor Calculus and Continuum Mechanics, Trafford Publishing, 2001.
[76] W. Nowacki, Theory of Asymmetric Elasticity, Pergamon Press, Oxford, 1986. Polish original 1971.
[77] P. Neff, The Cosserat couple modulus for continuous solids is zero viz the linearized Cauchy-stress tensor is symmetric, Z. Angew. Math. Mech. 86 (2006) 892–912. <http://www3.mathematik.tu-darmstadt.de/fb/mathe/bibliothek/preprints.html>.
[78] Martin H. Saad, Elasticity: Theory, Application and Numerics, Elsevier Butterworth, Heinemann, 2005.
[79] J. Jeong, H. Adib-Ramezani, M. Al-Mukhtar, Numerical simulation of elastic linear micropolar media based on the pore space length scale assumption, Strength Mater. 40 (2008) 425–438, doi:10.1007/s11223-008-9052-9.
[80] R.S. Lakes, Viscoelastic Solids, Mechanical Engineering Series, first ed., vol. 137, CRC Press, Boca Raton, 1999.
[81] Wenxing Haung, Erich Bauer, Numerical investigations of shear localization in a micropolar hypoplastic material, Int. J. Numer. Anal. Methods Geomech. 27 (4) (2003) 325–352.
[82] P. Neff, I. Münch, Constitutive modeling and FEM for a nonlinear Cosserat continuum, Proc. Appl. Math. Mech. (2006).
[83] Jena Jeong, Hamidréza Ramézani, Implementation of the finite isotropic linear cosserat models based on the weak form, in: Scientific committee of European Comsol Conference in Hannover, Germany, European Comsol Users Conference 2008, November 2008.
[84] P. Neff, J. Jeong, I. Münch, H. Ramézani, Linear Cosserat elasticity, conformal curvature and bounded stiffness, in: G.A. Maugin, V.A. Metrikine (Eds.), Mechanics of Generalized Continua One hundred Years After the Cosserats, Advances in Mechanics and Mathematics, vol. 21, Springer, Berlin, 2010, pp. 55–63.

[85] Patrizio Neff, Jena Jeong, Hamidréza Ramézani, Subgrid interaction and micro-randomness – novel invariance requirements in infinitesimal gradient elasticity, Int. J. Solids Struct. 46 (25–26) (2009) 4261–4276.
[86] Patrizio Neff, Jena Jeong, Andreas Fischle, Stable identification of linear isotropic Cosserat parameters: bounded stiffness in bending and torsion implies conformal invariance of curvature, Acta Mech. 211 (3) (2010) 237–249.
[87] R.D. Gauthier, W.E. Jahsman, Bending of a curved bar of micropolar elastic material, ASME J. Appl. Mech. 43 (1976) 502–503.
[88] M. Baluch, J.E. Goldberg, S.L. Koh, Finite element approach to plane microelasticity, J. Struct. Div.-Am. Soc. Civil Eng. 98 (1972) 1957–1964.
[89] Nakamura Sachio, Robert Benedict, Roderic Lakes, Finite element method for orthotropic micropolar elasticity, Int. J. Eng. Sci. 22 (3) (1984) 319–330.
[90] P. Trovalusci, R. Masiani, Non-linear micropolar and classical continua for anisotropic discontinuous materials, Int. J. Solids Struct. 40 (5) (2003) 1281–1297.
[91] M.B. Rubin, B. Nadler, A new 3-d finite element method for nonlinear elasticity using the theory of a Cosserat point, Int. J. Solids Struct. 40 (2003) 4585–4614.
[92] C.S. Jog, Higher-order shell elements based on the Cosserat model, and their use in the topology design of strutures, Comput. Methods Appl. Mech. Eng. 193 (2004) 2191–2220.
[93] L. Li, S. Xie, Finite element method for linear micropolar elasticity and numerical study of some scale effects phenomena in MEMS, Int. J. Mech. Sci. 46 (2004) 571–1587.
[94] S. Diebels, H. Steeb, The size effect in foams and its theoretical and numerical investigation, Proc. R. Soc. London A 458 (2002) 2869–2883.
[95] S. Diebels, H. Steeb, Stress and couple stress in foams, Comput. Mater. Sci. 28 (2003) 714–722.
[96] E. Sharbati, R. Naghdabadi, Computational aspects of the Cosserat finite element analysis of localization phenomena, Comput. Mater. Sci. 38 (2006) 303–315.
[97] F.Y. Huang, B.H. Yan, J.L. Yan, D.U. Yang, Bending analysis of micropolar elastic beam using a 3-d finite element method, Int. J. Eng. Sci. 38 (2000) 275–286.
[98] B. Zastrau, Zur Berechnung orientierter Kontinua – Entwicklung einer Direktorentheorie und Anwendung der Finiten Elemente. Number 4/60 in Fortschrittberichte der VDI Zeitschriften. Verein Deutscher Ingenieure, VDI-Verlag GmbH, Düsseldorf, 1981.
[99] B. Zastrau, H. Rothert, Herleitung einer direktortheorie für kontinua mit lokalen krmmungseigenschaften, Z. Angew. Math. Mech. 61 (1981) 567–581.
[100] P. Grammenoudis, C. Tsakmakis, Finite element implementation of large deformation micropolar plasticity exhibiting isotropic and kinematic hardening effects, Int. J. Numer. Methods Eng. 62 (12) (2005) 1691–1720.
[101] Hamidréza Ramézani, Jena Jeong, Environmentally motivated modeling of hygro-thermally induced stresses in the layered limestone masonry structures: physical motivation and numerical modeling, Acta Mech. (2011) 1–31, doi:10.1007/s00707-011-0463-5.
[102] P. Neff, J. Jeong, I. Münch, H. Ramézani, Mean field modeling of isotropic random Cauchy elasticity versus microstretch elasticity, Z. Angew. Math. Phys. 60 (3) (2009) 479–497.